TYPE Original Research
PUBLISHED 24 November 2025
DOI 10.3389/feart.2025.1664716



OPEN ACCESS

EDITED BY Hossein Azizi, University of Kurdistan, Iran

REVIEWED BY

Mohamed Faisal, Suez Canal University, Egypt Alexander U. Falster, Maine Mineral and Gem Museum, United States

*CORRESPONDENCE
Wei Guo,

№ 1907729905@qq.com

RECEIVED 12 July 2025 REVISED 19 September 2025 ACCEPTED 24 October 2025 PUBLISHED 24 November 2025

CITATION

Cui J, Guo W, Ren J, Ren Z, Song H and Liu G (2025) Mesoproterozoic post-orogenic magmatism on the southwestern North China Craton: onset of Columbia breakup. *Front. Earth Sci.* 13:1664716. doi: 10.3389/feart.2025.1664716

COPYRIGHT

© 2025 Cui, Guo, Ren, Ren, Song and Liu. This is an open-access article distributed under the terms of the Creative Commons
Attribution License (CC BY). The use, distribution or reproduction in other forums is permitted, provided the original author(s) and the copyright owner(s) are credited and that the original publication in this journal is cited, in accordance with accepted academic practice. No use, distribution or reproduction is permitted which does not comply with these terms.

Mesoproterozoic post-orogenic magmatism on the southwestern North China Craton: onset of Columbia breakup

Junping Cui^{1,2}, Wei Guo^{1*}, Junfeng Ren³, Zhanli Ren^{1,2}, Haoyu Song¹ and Guoqing Liu¹

¹Department of Geology, Northwest University, Xi'an, China, ²State Key Laboratory of Continental Evolution and Early Life, Department of Geology, Northwest University, Xi'an, China, ³Exploration and Development Research Institute of PetroChina Changqing Oilfield Company, Xi'an, China

Introduction: The North China Craton experienced multiple episodes of Mesoproterozoic anorogenic magmatism, which provides critical insights into the breakup process of the Columbia supercontinent. While numerous previous studies have focused on the southern and eastern margins of the craton, the southwestern margin remains relatively understudied, and its tectonic setting is still poorly constrained.

Methods: To investigate the tectonic context of Mesoproterozoic magmatic events along the southwestern margin and their relationship with the breakup of Columbia, this study presents a systematic analysis of the petrology, zircon U–Pb geochronology, and geochemistry of the granite porphyry in the Qi'angou area of Longxian, southwestern North China Craton.

Results: These data are integrated with geochemical characteristics of other Mesoproterozoic igneous rocks from the western margin to comprehensively analyze the magmatic activity in this region. Zircon U–Pb dating yielded an emplacement age of 1794 ± 10 Ma for the Qi'angou granite porphyry, indicating its formation during the Mesoproterozoic. Geochemical data show that the granite porphyry is peraluminous and belongs to the A2-type granite suite. It is enriched in large-ion lithophile elements (LILE) and depleted in high-field-strength elements (HFSE), with high Rb/Sr ratios (2.95–3.55), pronounced negative Eu anomalies, and low Mg# values, suggesting a crustal derivation.

Discussion: Combined with previous studies on coeval intermediate-mafic rocks (1740–1804 Ma)—including calc-alkaline basaltic andesites and high-K calc-alkaline diabases—these findings indicate that the North China Craton underwent extension during the late Paleoproterozoic to early Mesoproterozoic. Upwelling of a mantle plume beneath the southwestern margin triggered lithospheric thinning and partial melting of the upper crust, leading to a series of magmatic events. Comprehensive geochemical features and regional tectonic analysis suggest that the western margin igneous assemblage formed in a post-orogenic intracontinental extensional setting. This represents the initial geological record of the global breakup of the Columbia supercontinent within the North China Craton and provides key chronological

constraints for understanding the geodynamic mechanisms of supercontinental fragmentation.

KEYWORDS

North China Craton, mesoproterozoic, igneous rocks, post-orogenic extension, supercontinent breakup

1 Introduction

The North China Craton (NCC), an ancient continental nucleus formed at ~3.8 Ga, underwent multistage tectonic evolution (Wu and Zhong, 1998; Zhai, 2004; Zhao and Zhai, 2013). Previous studies have suggested that the basement of the North China Craton was formed by the assembly of multiple micro-continental blocks at approximately 2.5 Ga, which can be divided into six blocks: the Jiaoliao, Qianhuai, Xuchang, Fuping, Jining, and Alxa blocks (Zhai et al., 2005; Zhai and Santosh, 2011). During 2.25-2.0 Ga, three major rift systems developed in its northwestern, central, and northeastern-eastern sectors. These rift basins subsequently evolved into oceanic basins and initiated subduction processes (Santosh, 2010; Zhai and Santosh, 2011; Zhai et al., 2021). Following prolonged subduction-accretion, the craton achieved final cratonization through continental collisions during 1.97-1.82 Ga, forming three principal suture zones: the Khondalite Belt (north), Trans-North China Orogen (central), and Jiao-Liao-Ji Belt (east) (Zhai and Peng, 2007; Santosh et al., 2011; Liu et al., 2025).

At approximately 1.8 Ga, following the final cratonization of the North China Craton, a series of post-orogenic tectonic activities commenced, leading to multiple episodes of anorogenic magmatism and the formation of various igneous rocks. These anorogenic magmatic events were primarily distributed along the southern and northern margins as well as the central region of the craton. This period is characterized by the Xiong'er Group volcanic rocks on the southern margin of the North China Craton, ong with their coeval intrusive rocks and the mafic dike swarms in the Wutai and Hengshan areas of the northern craton, were closely associated with contemporaneous extensional tectonism. While previous studies have extensively analyzed these magmatic events, research on the southwestern margin of the craton remains limited, with relatively scarce information on the tectonic setting of the Mesoproterozoic magmatic events in this area (Zhao et al., 2001; Zhao et al., 2004; Peng et al., 2004; Li et al., 2024; Lu et al., 2002; Zhai et al., 2014; Xiang, 2014; Huang et al., 2020).

Simultaneously, the Mesoproterozoic magmatic events in the craton may be related to the global breakup of the Columbia supercontinent (Zhao et al., 2001; Zhao et al., 2004; Peng et al., 2004; Li et al., 2024). The extensional breakup of supercontinents is often accompanied by various types of anorogenic magmatism. Volcanic rocks are typically characterized by bimodal assemblages, while intrusive rocks are represented by anorthosite-mangerite-charnockite-granite (AMCG) suites, rapakivi granites, and mafic dike swarms (Hou et al., 2008; Ernst et al., 2016; Geng et al., 2019). However, the nature and tectonic setting of these geological events remain controversial (e.g., rift, mantle plume, post-collision, and island arc settings). The lack of tectonic activity information from the southwestern margin is critical for clarifying the early Mesoproterozoic tectonic evolution of the North China Craton and

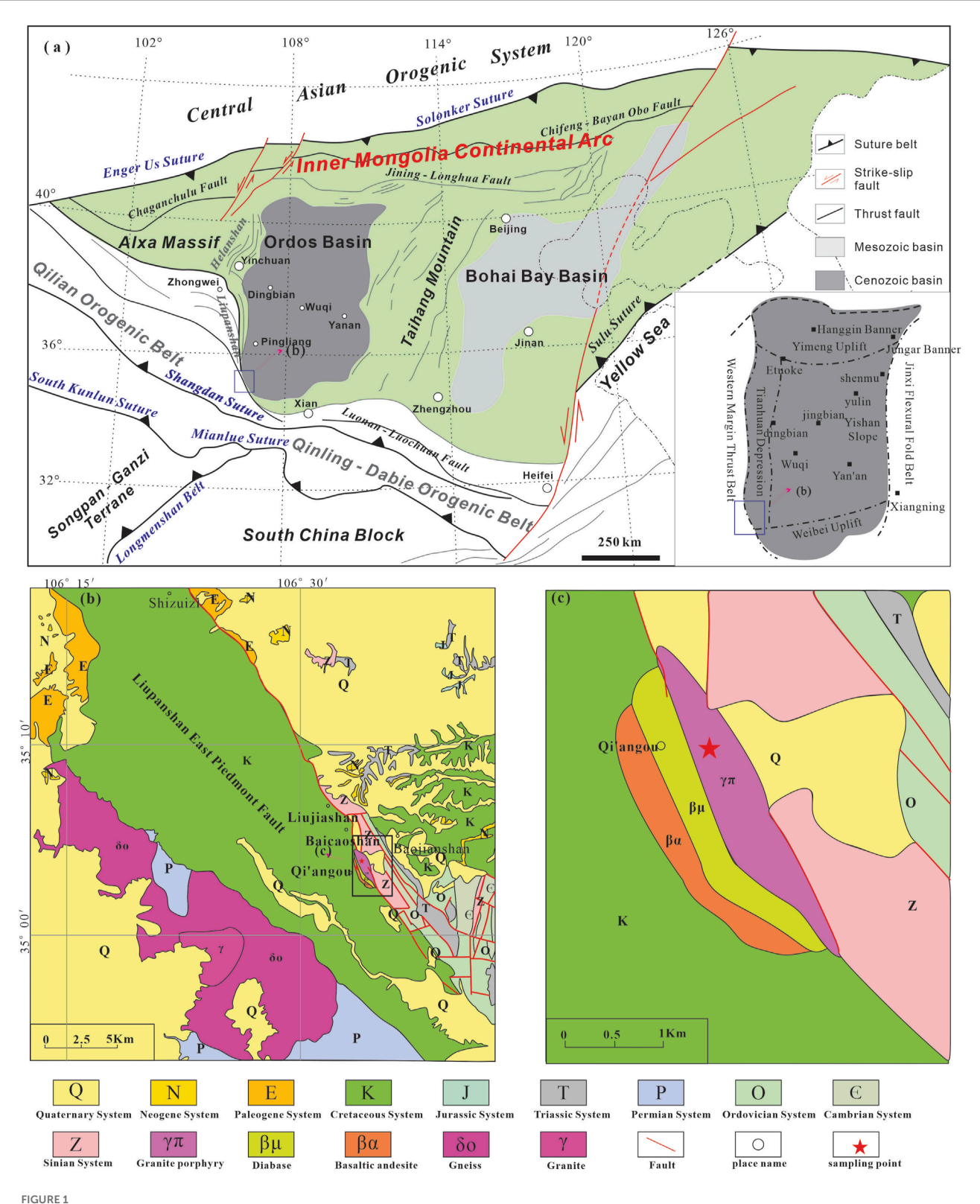
its relationship with the breakup of the Columbia supercontinent (Zhai et al., 2014; Xiang, 2014; Xiang et al., 2020; Geng et al., 2019). Clearly, elucidating the nature and dynamic mechanisms of the tectonic events between 1.8 and 1.6 Ga along the southwestern margin of the North China Craton is of significant scientific importance for understanding the transition from basement to cover tectonic regimes and for comparing with typical cratons worldwide.

The western margin of the North China Craton also experienced typical anorogenic magmatic activities during the Mesoproterozoic, concentrated around 1.80–1.75 Ga (Xu et al., 2014; Xu et al., 2017; Xu et al., 2019; Gao et al., 2013; Gao et al., 2023). This study focuses on the granitic porphyry in the Qi'angou area of Longxian County on the western margin of the North China Craton. Through petrological characteristics, geochemical composition, and zircon U-Pb dating analysis, we aim to determine its genetic mechanism and formation age. Additionally, by integrating geochemical features of other Mesoproterozoic igneous rocks from the western margin (Xu et al., 2014; Xu et al., 2019; Gao et al., 2013; Gao et al., 2023), we seek to analyze the tectonic evolution of the western North China Craton–Ordos Block during the Mesoproterozoic and its magmatic response to the breakup of the Columbia supercontinent.

2 Geological setting and petrological characteristics

The Ordos Basin is located in the western part of the North China Craton (NCC). During the Middle to Late Ordovician, the North China Block experienced uplift, leading to the termination of the epicontinental sea depositional system in the basin. The seawater gradually retreated northward and eastward, resulting in the development of a transitional depositional system characterized by marine-terrestrial interactions by the Late Carboniferous. In the Early Permian, the oceanic crusts from both the northern and southern margins subducted beneath the North China Block, forming a tectonic framework in the basin characterized by uplifts on the northern and southern margins and a central depression. It can be divided into six first-order tectonic units: the Yimeng Uplift, the Western Margin Thrust Belt, the Tianhuan Depression, the Yishan Slope, the Jinxi Flexural Fold Belt, and the Weibei Uplift (Luo et al., 2024; Jiang et al., 2024; Yang et al., 2000; He, 2022; Zhao et al., 2025).

The periphery of the basin is controlled by Cenozoic graben systems, bordered by the Yinshan Orogenic Belt to the north, the Qinling Orogenic Belt to the south, the Lvliangshan Structural Belt to the east, and the Helan-Liupanshan Thrust Belt to the west, forming a typical basin-mountain coupling system. The basin developed on an Archean to Paleoproterozoic crystalline basement and is classified as a large polycyclic superimposed basin (Zhao et al.,



Simplified geological map of major tectonic units in the North China Craton and adjacent areas (a) (modified from Tao et al., 2025; Sun and Dong, 2019) and simplified geological maps of Qi'angou and adjacent areas (b,c) (after 1:200,000 Longxian Sheet).

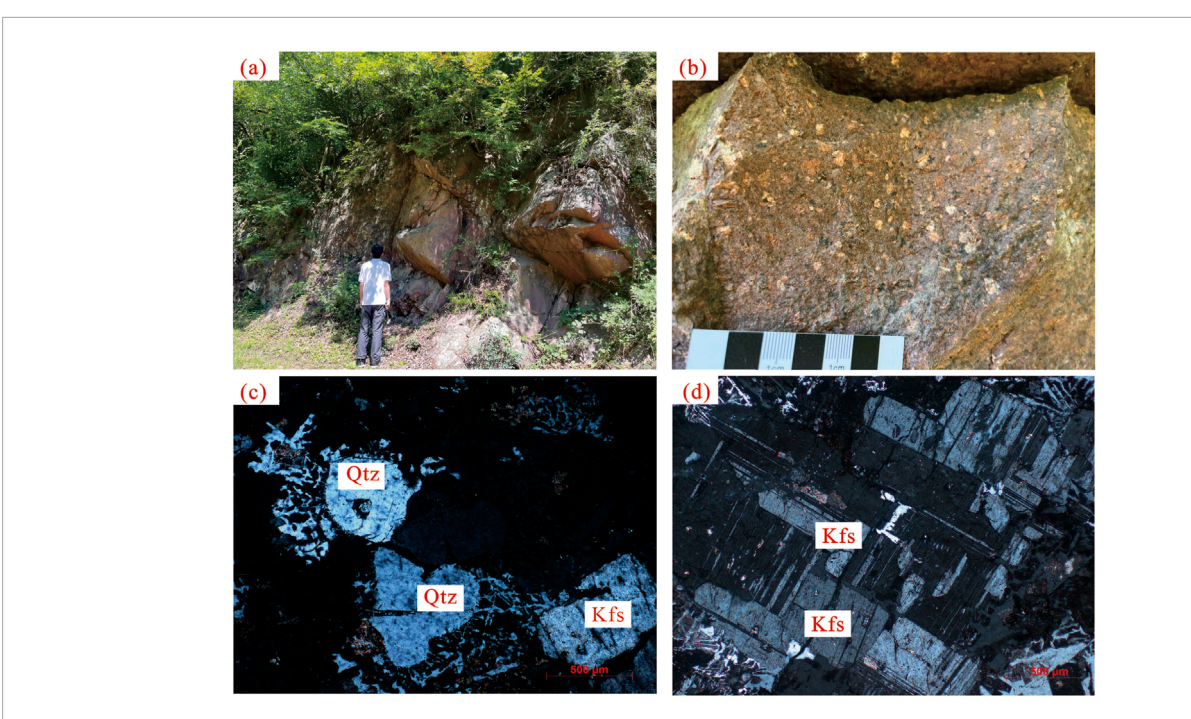
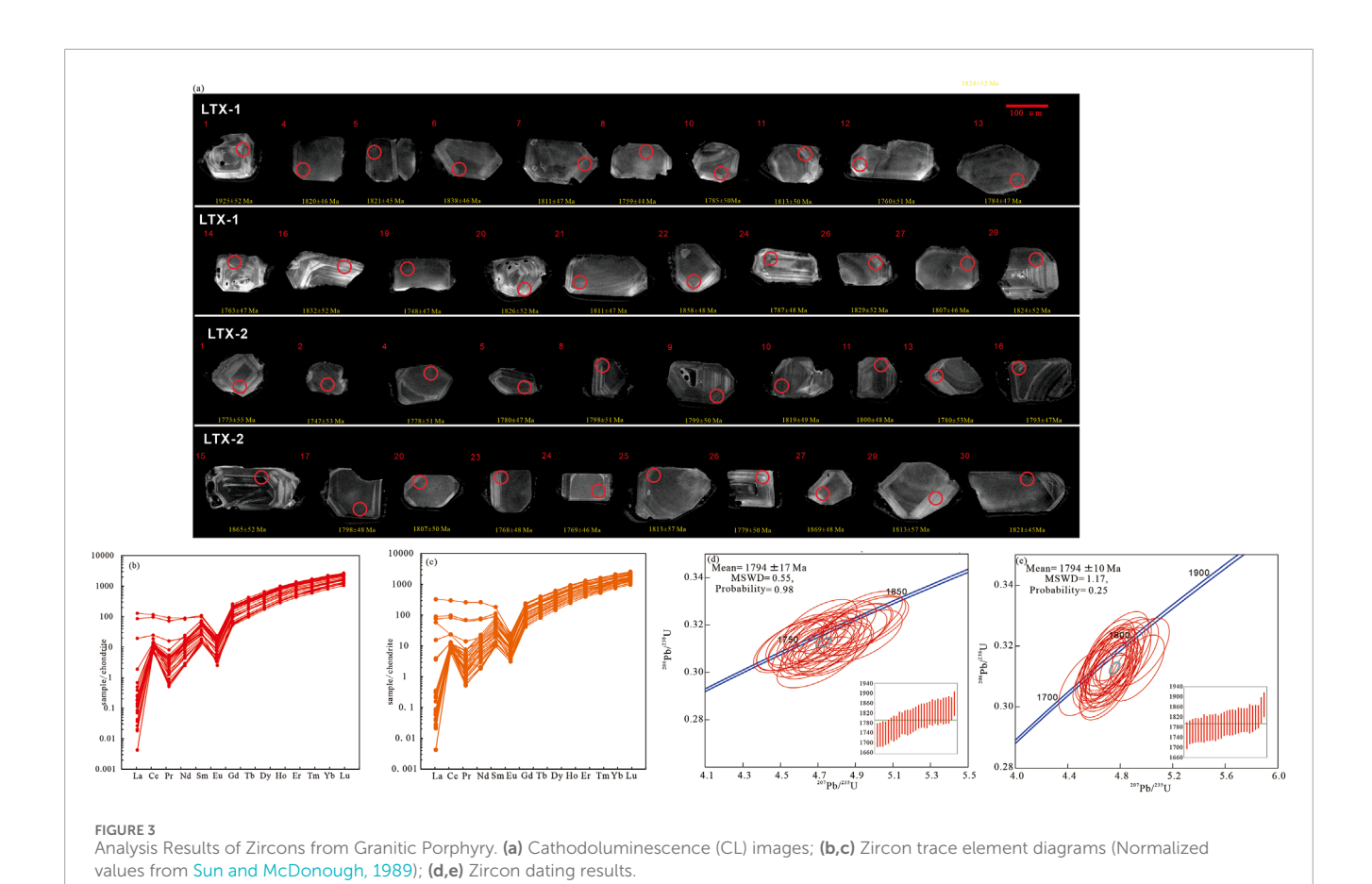
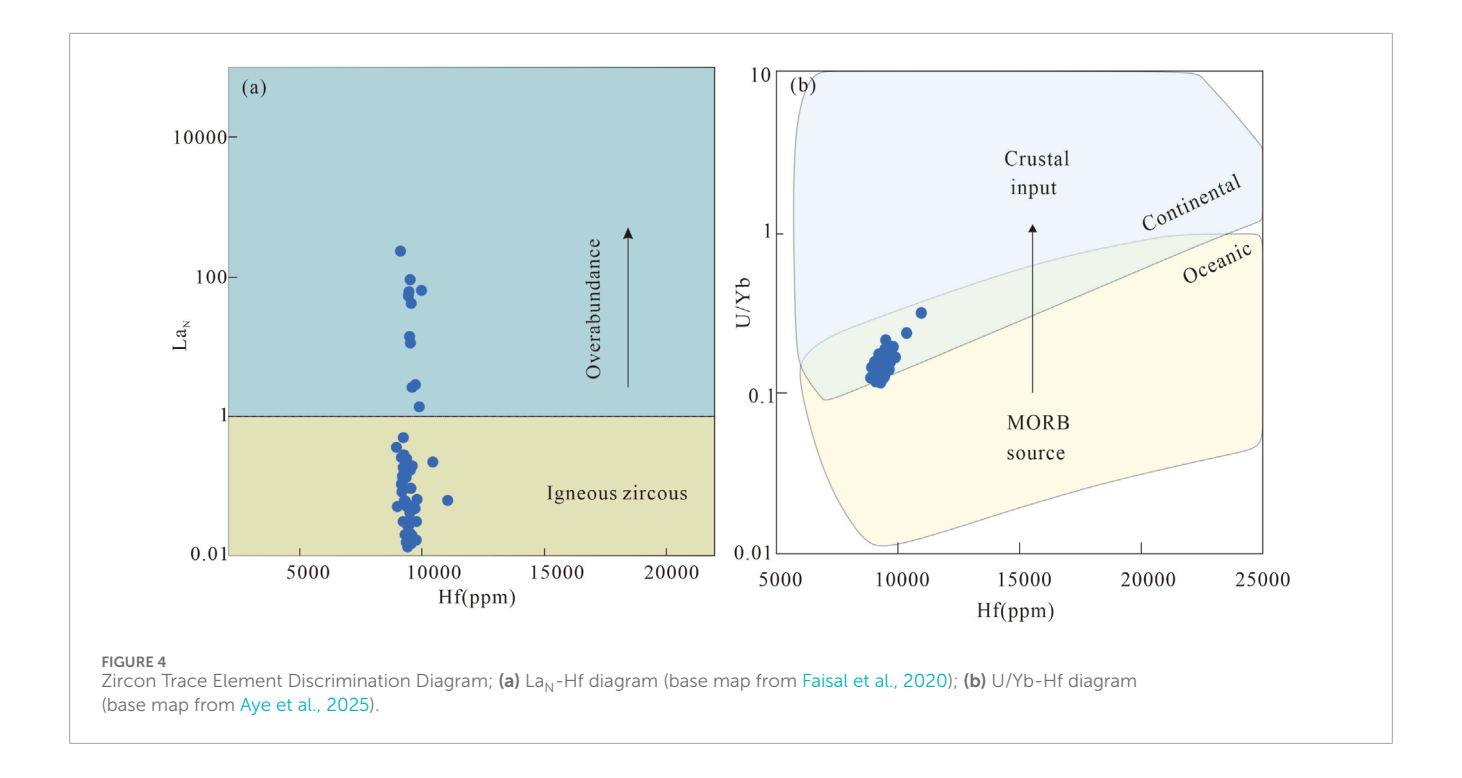


FIGURE 2
Field and microscopic photos of Qi'angou granite porphyry Field photos: (a), (b) Microscopic photos: (c), (d) Qtz = quartz; Kfs = K-feldspar.





2025; He, 2022). Its sedimentary evolutionary sequence comprises five major stages: the Meso-Neoproterozoic rift trough stage, the Early Paleozoic shallow-water platform stage, the Late Paleozoic coastal plain stage, the Mesozoic inland lacustrine basin stage, and the Cenozoic peripheral fault depression stage (He, 2022; Liu G. Q. et al., 2024).

The internal structure of the basin is relatively simple, characterized by a monoclinal structure with a gentle westward dip (less than 3°). However, the basin margins exhibit more complex structural belts with varying trends and styles. Intense and heterogeneous orogenic activities have formed diverse basin-mountain coupling systems (Lin et al., 2016).

The study area is located in the Liupanshan region on the southwestern margin of the Ordos Basin (Figure 1a). The Liupanshan-Helanshan region has undergone multiple phases of tectonic deformation, including the Early Paleozoic, Indosinian, Yanshanian, and Himalayan orogenies. Its early evolution was controlled by the Qinling-Qilian-Helan triple-arm rift system, which developed from the Meso-Neoproterozoic to the Early Paleozoic (Zhang et al., 2006; Yao et al., 2025). During the Early Paleozoic orogeny, the area experienced folding under dextral shear. The Indosinian orogeny, driven by the subduction of the Tethyan Ocean, subjected the region to intense deformation. The present-day tectonic framework primarily formed during the Yanshanian and Himalayan movements (Li et al., 2013).

Sampling was conducted at Qian'gou, Longxian County within the southwestern Liupanshan Fault Zone (Figures 1b,c); coordinates: 35°03.674′N, 106°34.539′E, where intermediate-acidic igneous rocks are exposed. The analyzed samples represent granite porphyry. Field investigations reveal that the granite porphyry primarily occurs as dikes or irregular blocks with sporadic outcrops, exhibiting a zonal distribution pattern in the region. It is surrounded by Lower Cretaceous purplish-red sandstones and mudstones,

as well as Sinian carbonate rocks. Quaternary cover obscures the spatial relationships at rock mass-host rock interfaces. The porphyry displays significant surface weathering, though fresh surfaces are exposed along fractures. Macroscopically, it exhibits a pinkish hue with medium-fine grained granitic to porphyritic textures and massive structure (Figures 2a,b). Phenocrysts account for approximately 35% of the total rock volume, with potassium feldspar (20%) displaying obvious alteration features, quartz (10%) presenting corrosion textures characterized by intact pristine cores and dissolved margins, and plagioclase (5%) showing no distinct special textures (or supplement specific features if available). The groundmass consists predominantly of quartz and feldspar with minor mafic minerals, displaying fine-grained to microcrystalline textures (Figures 2c,d). Based on structural characteristics, textural relationships, and mineral composition, the rock is classified as granite porphyry.

3 Analytical methods

3.1 Zircon mount preparation and cathodoluminescence (CL) imaging

The samples collected from field outcrops were first cleaned and cut to remove impurities and weathered exteriors. Subsequently, zircon grain separation was carried out in the laboratory. Zircon grain separation: First, the bulk rock is crushed and then sieved to obtain particles of the target size range. Zircon grains are subsequently separated by leveraging their high density as well as their non-magnetic or very weakly magnetic properties. Zircons with intact crystal forms, few or no cracks, high transparency, and no inclusions were selected for target preparation. The preparation work was conducted at the State Key Laboratory of Evolution and

TABLE 1 LA-ICP-MS zircon U-Pb dating results of granitic porphyry (LTX-1).

Point	nt Th U Pb Th				Isotope ratio					Age						
		(10 ⁻⁶)			²⁰⁷ Pb/ ²⁰⁶ Pb	1σ	²⁰⁷ Pb/ ²³⁵ U	1 σ	²⁰⁶ Pb/ ²³⁸ U	1σ	²⁰⁷ Pb/ ²⁰⁶ Pb	1σ	²⁰⁷ Pb/ ²³⁵ U	1σ	²⁰⁶ Pb/ ²³⁸ U	1σ
01	23.5	14.85	10.07	0.63	0.1121	0.0034	4.9524	0.1523	0.3205	0.0075	1834	53	1811	26	1792	38
02	47.32	41.48	21.05	0.88	0.1117	0.0028	4.9012	0.1309	0.3182	0.0073	1828	45	1803	23	1781	36
03	46.38	46.14	21.20	0.99	0.1116	0.0029	4.8899	0.1324	0.3179	0.0073	1826	46	1803	23	1780	36
04	44.94	39.51	19.70	0.88	0.1113	0.0028	4.7903	0.1286	0.3123	0.0071	1821	46	1783	23	1752	35
05	39.5	35.23	17.18	0.89	0.1124	0.0029	4.7902	0.1290	0.3092	0.0071	1838	46	1783	23	1737	35
06	36.51	26.03	15.41	0.71	0.1107	0.0029	4.7229	0.1296	0.3095	0.0071	1811	47	1771	23	1738	35
07	48.69	45.29	21.42	0.93	0.1076	0.0027	4.6157	0.1202	0.3113	0.0071	1759	44	1752	21	1747	35
08	27.66	21.91	11.76	0.79	0.1064	0.0030	4.5736	0.1323	0.3118	0.0072	1739	50	1745	24	1749	35
09	25.58	16.86	10.87	0.66	0.1091	0.0031	4.7977	0.1398	0.3190	0.0074	1785	50	1785	25	1785	36
10	27.1	17.32	11.67	0.64	0.1108	0.0031	4.9325	0.1438	0.3230	0.0075	1813	50	1808	25	1804	37
11	27.35	18.17	11.42	0.66	0.1077	0.0030	4.6411	0.1360	0.3128	0.0072	1760	51	1757	26	1754	36
12	39.12	33.62	17.16	0.86	0.1091	0.0029	4.7028	0.1290	0.3128	0.0072	1784	47	1768	23	1754	36
13	41.69	38.13	18.48	0.91	0.1078	0.0028	4.6753	0.1278	0.3146	0.0072	1763	47	1763	23	1763	35
14	41.75	37.29	18.24	0.89	0.1061	0.0028	4.5433	0.1236	0.3106	0.0071	1734	47	1739	23	1744	35
15	25.5	17.82	10.48	0.70	0.1120	0.0033	4.6949	0.1410	0.3043	0.0071	1831	52	1767	25	1712	35
16	39.26	34.6	17.10	0.88	0.1100	0.0029	4.6979	0.1287	0.3099	0.0071	1799	47	1767	23	1740	35
17	45.15	42.05	20.08	0.93	0.1066	0.0027	4.6097	0.1236	0.3138	0.0071	1742	46	1751	22	1759	35
18	45.34	39.74	20.15	0.88	0.1069	0.0028	4.7125	0.1288	0.3198	0.0073	1748	47	1770	23	1789	36
19	23.71	15.19	10.25	0.64	0.1116	0.0033	4.9423	0.1490	0.3213	0.0075	1826	52	1810	26	1796	37
20	37.57	34.47	16.63	0.92	0.1107	0.0029	4.7493	0.1314	0.3112	0.0071	1811	47	1776	23	1747	35
21	35.62	30.4	15.75	0.85	0.1136	0.0031	4.9400	0.1387	0.3154	0.0073	1858	48	18,090	24	1767	36
22	41.67	38.86	18.56	0.93	0.1096	0.0029	4.7652	0.1311	0.3153	0.0072	1793	47	1779	23	1767	35
23	40.15	34.76	17.72	0.87	0.1093	0.0029	4.7322	0.1308	0.3142	0.0072	1787	47	1773	23	1762	35
24	30.52	20.4	13.07	0.67	0.1086	0.0031	4.7255	0.1386	0.3157	0.0073	1776	51	1772	25	1769	36
25	27.52	17.33	11.45	0.63	0.1118	0.0033	4.7788	0.1434	0.3100	0.0072	1829	52	1781	25	1741	36
26	46.16	41.53	20.14	0.90	0.1105	0.0029	4.6876	0.1268	0.3078	0.0070	1807	46	1765	23	1730	35
27	78.79	49.24	32.33	0.62	0.1089	0.0026	4.6302	0.1156	0.3085	0.0069	1781	42	1755	21	1733	34
28	27	18.3	11.46	0.68	0.1115	0.0032	4.8491	0.1448	0.3155	0.0073	1824	52	1794	25	1768	36

(Continued on the following page)

TABLE 1 (Continued) LA-ICP-MS zircon U-Pb dating results of granitic porphyry (LTX-1).

Point	nt Th U Pb Th/U					Isotope ratio						Age					
		(10 ⁻⁶)			²⁰⁷ Pb/ ²⁰⁶ Pb	1σ	²⁰⁷ Pb/ ²³⁵ U	1σ	²⁰⁶ Pb/ ²³⁸ U	1σ	²⁰⁷ Pb/ ²⁰⁶ Pb	1σ	²⁰⁷ Pb/ ²³⁵ U	1σ	²⁰⁶ Pb/ ²³⁸ U	1σ	
29	38.99	29.28	16.66	0.75	0.1063	0.0028	4.5623	0.1259	0.3114	0.0071	1737	48	1742	23	1748	34.9	
01	30.62	23.7	13.47	0.77	0.1086	0.0033	4.7873	0.1505	0.3199	0.0075	1775	55	1783	26	1789	37	
02	49.45	48.21	22.50	0.97	0.1077	0.0028	4.7170	0.1269	0.3178	0.0072	1760	46	1770	23	1779	35	
03	28.13	19.9	12.07	0.71	0.1087	0.0031	4.7225	0.1391	0.3151	0.0073	1778	51	1771	25	1766	36	
04	41.28	35.09	18.06	0.85	0.1088	0.0028	4.6903	0.1273	0.3127	0.0071	1780	47	1766	23	1754	35	
05	31.12	21.51	13.28	0.69	0.1092	0.0030	4.7335	0.1344	0.3146	0.0072	1785	49	1773	24	1763	35	
06	26.73	16.65	11.25	0.62	0.1099	0.0031	4.8238	0.1410	0.3183	0.0074	1798	51	1789	25	1781	36	
07	30.74	23.05	13.23	0.75	0.1100	0.0031	4.7695	0.1388	0.3146	0.0073	1799	50	1780	24	1763	36	
08	34.35	28.72	14.75	0.84	0.1112	0.0030	4.6949	0.1334	0.3064	0.0070	1819	49	1766	24	1723	35	
09	40.78	34.82	17.96	0.85	0.1100	0.0029	4.7323	0.1315	0.3120	0.0071	1800	48	1773	23	1751	35	
10	40.58	39.23	18.34	0.97	0.1082	0.0029	4.7176	0.1303	0.3162	0.0072	1770	48	1770	23	1771	35	
11	26.94	18.8	11.27	0.70	0.1088	0.0032	4.6547	0.1424	0.3103	0.0072	1780	53	1759	26	1741	36	
12	39.67	27.32	16.93	0.69	0.1079	0.0029	4.6888	0.1299	0.3151	0.0072	1765	48	1765	23	1766	35	
13	34.46	28.23	15.34	0.82	0.1129	0.0033	4.9488	0.1488	0.3180	0.0074	1847	52	1811	25	1780	36	
14	43.63	41.65	19.87	0.95	0.1096	0.0029	4.7894	0.1315	0.3169	0.0072	1793	47	1783	23	1775	35	
15	38.97	34.58	17.08	0.89	0.1099	0.0029	4.6982	0.1299	0.3102	0.0071	1798	48	1767	23	1741	35	
16	27.04	16.48	11.27	0.61	0.1109	0.0032	4.7501	0.1410	0.3108	0.0072	1814	51	1776	25	1745	35	
17	35.63	27.72	15.56	0.78	0.1086	0.0029	4.7102	0.1318	0.3147	0.0072	1776	48	1769	23	1764	35	
18	29.16	20.51	12.22	0.70	0.1105	0.0031	4.7096	0.1367	0.3093	0.0071	1807	50	1769	24	1737	35	
19	35.9	28.67	15.45	0.80	0.1105	0.0030	4.7298	0.1315	0.3105	0.0071	1808	48	1773	23	1743	35	
20	24.82	14.94	10.17	0.60	0.1069	0.0031	4.5374	0.1367	0.3079	0.0071	1747	53	1738	25	1730	35	
21	36.64	29.82	15.83	0.81	0.1081	0.0029	4.6519	0.1282	0.3121	0.0071	1768	48	1759	23	1751	35	
22	41.56	40.77	18.72	0.98	0.1082	0.0028	4.6619	0.1257	0.3127	0.0071	1767	46	1760	23	1754	35	
23	39.66	36.09	17.41	0.91	0.1106	0.0029	4.6799	0.1272	0.3071	0.0070	1808	47	1764	23	1727	34	
24	30.57	22.62	13.13	0.74	0.1088	0.0030	4.7005	0.1354	0.3134	0.0072	1779	50	1767	24	1758	35	
25	33.29	21.74	14.19	0.65	0.1143	0.0031	4.9275	0.1379	0.3128	0.0072	1869	48	1807	24	1754	35	
26	45.95	30.27	19.34	0.66	0.1105	0.0029	4.7576	0.1284	0.3123	0.0071	1808	46	1777	23	1752	35	
27	20.95	11.69	8.84	0.56	0.1109	0.0036	4.8515	0.1589	0.3175	0.0075	1813	57	1794	28	1778	37	
28	58.28	50.66	25.97	0.87	0.1113	0.0028	4.8383	0.1283	0.3153	0.0071	1821	45	1792	22	1767	35	

TABLE 2 Composition of major, trace and rare earth elements of the granite porphyry.

Sample	24LXT- 1	24LXT- 2		24LXT- 1	24LXT- 2					
Major element (%)										
SiO ₂	70.96	70.48	Cs	0.71	0.65					
Al_2O_3	12.63	12.36	Ва	1,253	1,311					
TFe ₂ O ₃	4.23	4.35	Hf	19.1	19.5					
MgO	0.891	0.909	Ta	1.92	1.58					
CaO	0.300	0.599	W	0.93	0.68					
Na ₂ O	1.87	2.74	Tl	0.70	0.57					
K ₂ O	6.52	5.83	Pb	2.94	2.85					
MnO	0.043	0.045	Bi	0.011	0.015					
P_2O_5	0.093	0.088	Th	12.7	12.3					
TiO ₂	0.509	0.508	U	2.68	2.09					
LOI	1.73	1.85	Cr	12.2	12.0					
Trace elemen	ts (ppm)		Rare earth elements (ppm)							
Li	10.2	11.6	Y	99.7	87.1					
Be	2.92	3.03	La	177	176					
Sc	18.3	8.46	Се	391	336					
V	5.28	4.59	Pr	41.3	38.2					
Со	2.29	2.23	Nd	152	142					
Ni	5.15	4.65	Sm	27.5	25.0					
Cu	16.4	13.5	Eu	4.26	3.94					
Zn	73.4	75.0	Gd	22.0	20.4					
Ga	24.2	25.2	Tb	3.47	3.16					
Rb	144	125	Dy	18.9	16.6					
Sr	40.6	42.4	Но	3.59	3.11					
Zr	845	875	Er	10.02	8.86					
Nb	36.1	35.9	Tm	1.57	1.40					
Мо	0.58	0.43	Yb	9.61	8.76					
In	0.11	0.10	Lu	1.55	1.46					

Early Life, Northwest University, using a high-vacuum analytical scanning electron microscope (JSM-EST 100) equipped with the GATAN MINICL system produced by Gatan, United States, for CL imaging. During imaging, use lens tissue or other lint-free and soft paper dampened with anhydrous ethanol to wipe the

polished sample mount surface once to remove polishing residue and other contaminants. When photographing, select an appropriate magnification based on the purpose and the size of the zircon grains, and ensure that the overall arrangement direction of the zircon grains in a given sample is aligned either horizontally or vertically relative to the microscope's orientation.

Zircon U-Pb dating analysis was also performed at the State Key Laboratory of Evolution and Early Life, Northwest University, using LA-ICP-MS as the analytical instrument. The U-Pb dating of zircon was conducted using the international standard zircon 91,500 as an external standard for calibration. The standard was measured once every 4–5 sample analysis points to ensure consistent instrumental conditions between the standard and the samples. Before and after every 20 zircon analyses, NIST SRM610 was measured twice each time, with Si used as an internal standard to determine the contents of U, Th, and Pb in zircon. Detailed experimental procedures for zircon U-Pb dating can be found in references (Song et al., 2002; Yuan et al., 2003).

3.2 Major and trace element analysis

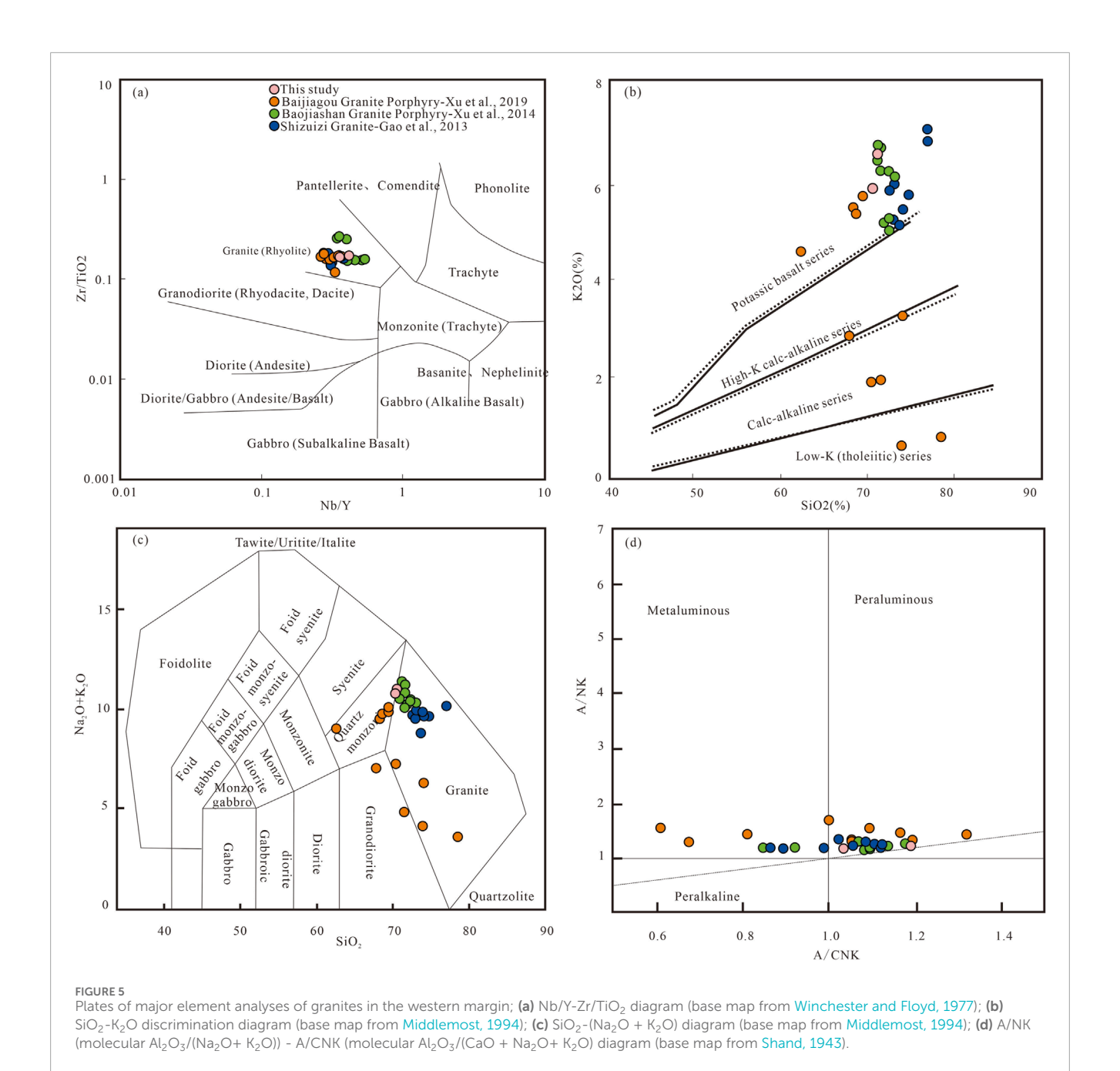
Fresh rock samples were pulverized to <75 μ m (<200 mesh) using an agate mortar. Major elements were determined by X-ray fluorescence spectrometry (XRF; Rigaku RIX 2100) on fused glass beads. Analytical accuracy (better than 1%) and precision (<5% RSD) were monitored using certified reference materials BCR-2 and GBW07105. Trace elements were analyzed by inductively coupled plasma–mass spectrometry (ICP-MS; Agilent 7500a) following a dual-digestion protocol. The dissolution of the samples is achieved through a combination of open-vessel decomposition using 1.5 mL of HNO3, 1.5 mL of HF, and 0.02 mL of HClO4, as well as closed high-pressure vessel decomposition using HNO3 and HF. The standard samples are selected from international reference materials BHVO-1, BCR-2, and AGV-1. For most trace elements, the analytical error is less than 2%, and the accuracy is better than 10%.

4 Analytical results

4.1 Zircon U-Pb geochronology of granite porphyry

Zircons separated from the Qiangou granite porphyry samples (LTX-1, LTX-2) are mostly colorless or light brown (Figure 3a), with a small number being darker in color. They are transparent to translucent, with grain sizes ranging from 100 to 150 μm and length-to-width ratios mostly between 1:1 and 1:2. The zircons are predominantly euhedral or subhedral prismatic crystals, and most exhibit oscillatory zoning.

The chondrite-normalized REE distribution patterns of the granite porphyry (Figures 3b,c) show that the granite porphyry is depleted in light rare earth elements (LREEs) ((La/Sm) $_{\rm N}$ <0.5) and enriched in heavy rare earth elements (HREEs) ((Gd/Yb) $_{\rm N}$ >2.0), with the distribution patterns being left-inclined. Meanwhile, in the LaN-Hf diagram, all zircon data points fall within the field of magmatic zircons (Figure 4a). The U/Yb-Hf ratios



of zircons (Figure 4b) can be used to discriminate their formation environments. As shown in the diagram, all data points plot within the continental zircon field, indicating that the granitic porphyry zircons primarily formed in a continental crustal environment.

The Th/U ratio is an important indicator for determining zircon genesis. Magmatic zircons typically exhibit higher Th/U ratios (Vavra et al., 1996; Yang and Wang, 2010; Faisal et al., 2025). The granite porphyry samples have relatively high Th/U values (Table 1), ranging from 0.56 to 0.99. Therefore, based on the Th/U ratios, the zircons in these samples are interpreted to be of magmatic origin (Vavra et al., 1996; Yang and Wang, 2010).

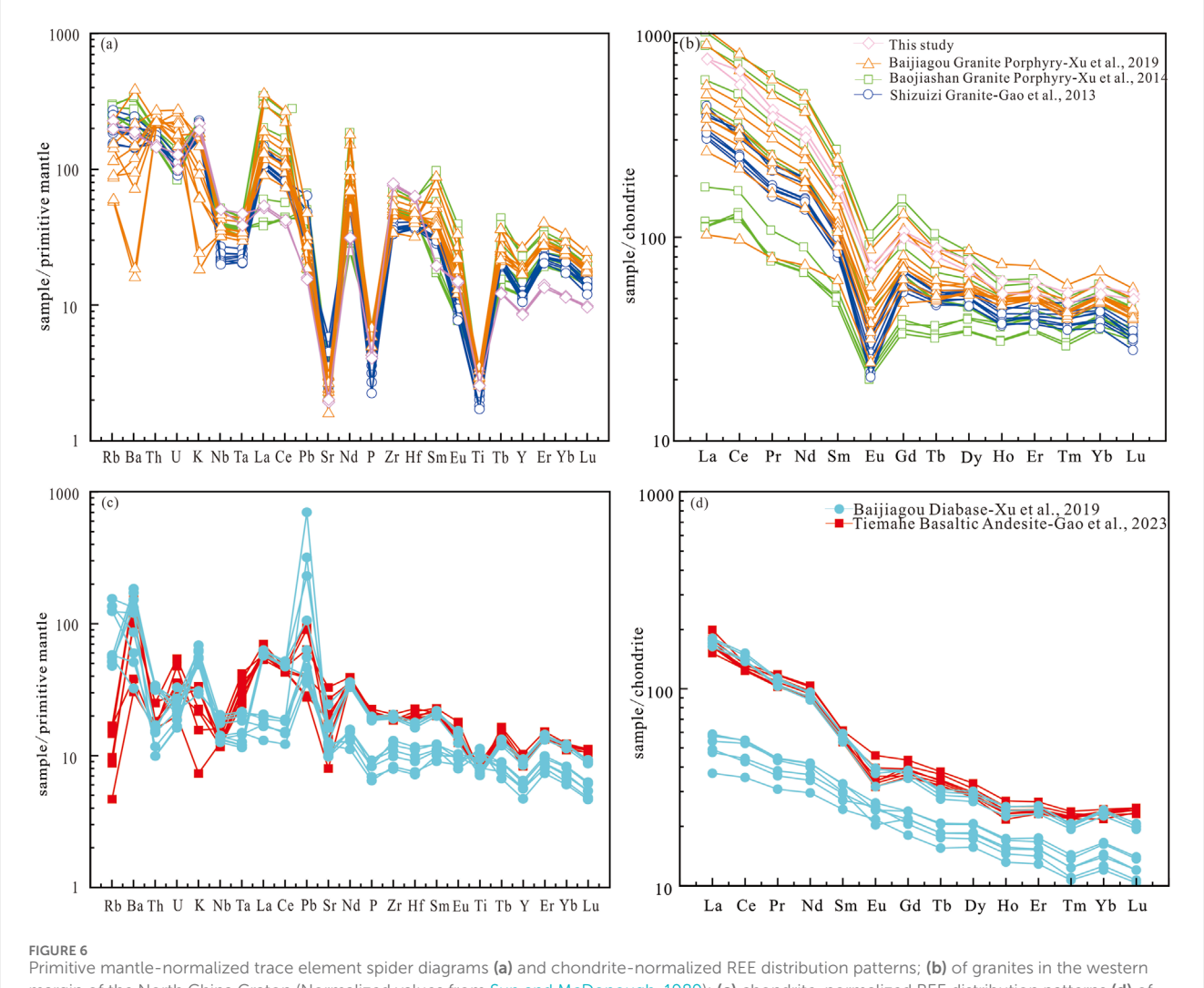
For zircon U-Pb dating, we employed 207 Pb/ 206 Pb ages for older zircons (>1 Ga) and 206 Pb/ 238 U ages for younger grains (<1 Ga) following established protocols (Black et al., 2003). The

two granite porphyry samples yielded weighted mean ages of 1794 \pm 17 Ma (MSWD = 0.55) and 1794 \pm 10 Ma (MSWD = 0.25), respectively (Figures 3d,e).

4.2 Whole-rock geochemical characteristics

4.2.1 Major element characteristics of granites in the southwestern margin

Due to the limited amount of research data in this study, the analysis integrates contemporaneously formed granite bodies from the early Mesoproterozoic era in the southwestern margin of the North China Craton, such as the Baojiashan granite porphyry (1781)



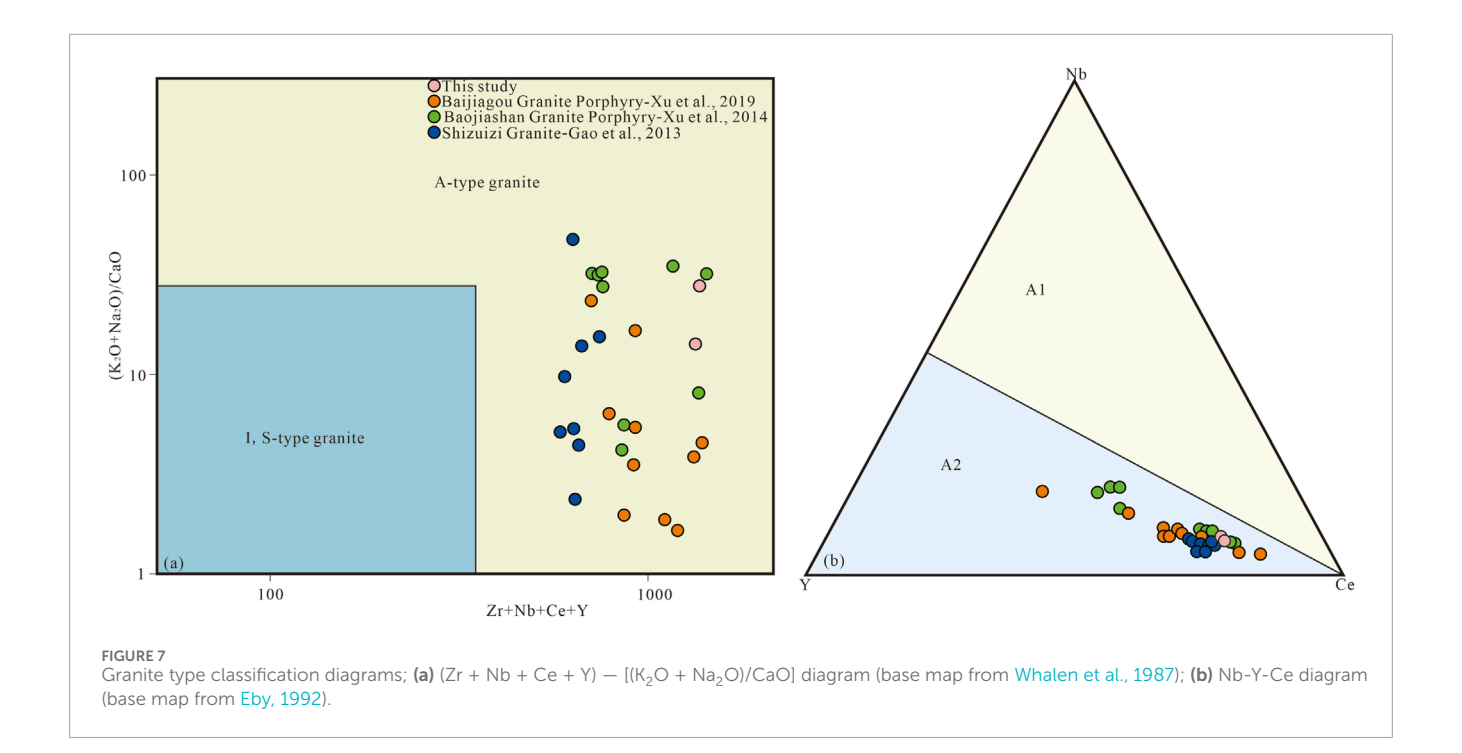
margin of the North China Craton (Normalized values from Sun and McDonough, 1989); (c) chondrite-normalized REE distribution patterns (d) of intermediate-mafic rocks in the western margin (Normalized values from Sun and McDonough, 1989).

 \pm 12 Ma), Baijiagou granite porphyry (1804 \pm 21 Ma), and Shizuizi granite (1792 \pm 16 Ma) (Xu et al., 2014; 2019; Gao et al., 2013).

The major element geochemical test results of the Qian'gou granite porphyry are shown in Table 2. By integrating the granite data from the entire southwestern margin of the North China Craton, it is found that the samples from Baojiashan, Shizuizi, and the Qian'gou in this study all exhibit characteristics of high silica (70.47%–76.69%) and potassium enrichment (4.95%–6.69%). The granite samples from the Baijiagou area show significant variations in SiO₂ content (62.02%-78.24%) and even greater variations in K₂O content (0.56%-5.65%). In the Nb/Y-Zr/TiO₂ diagram, all samples from various regions fall into the granite field (Figure 5a). In the SiO₂-(Na₂O + K₂O) diagram, the majority of the data points fall within the granite field (Figure 5c). In the SiO₂-K₂O diagram, the granite samples from Baojiashan, Qian'gou, and Shizuizi plot in the shoshonite field (Figure 5b), while the Baijiagou samples are distributed across different fields. Most of the granite samples have relatively high (A/CNK) values; both the Baojiashan granite porphyry and Qian'gou granite porphyry are peraluminous, and most samples from Shizuizi and Baijiagou are metaluminous (Figure 5d).

4.2.2 Trace and rare earth element characteristics of granites in the southwestern margin

The trace and rare earth element geochemical test results of the Qiangou granite porphyry are shown in Table 2. The primitive mantle-normalized diagram (Figure 6a) of the granites exhibits enrichment in LILEs (Rb, Ba, K) and depletion in HFSEs (Nb, Ti, P), with a significant negative Sr anomaly. The rocks have relatively high Rb/Sr ratios, which are much higher than those of I-type and S-type granitic rocks (0.61 and 1.81, respectively), similar to the geochemical characteristics of A-type granite porphyry (Whalen et al., 1987). The chondrite-normalized REE patterns (Figure 6b) are generally right-inclined, with enrichment in light rare earth elements (LREEs) and flat heavy rare earth elements (HREEs), showing obvious LREE/HREE fractionation. The average (La/Yb)_N is 8.91, with a significant Eu anomaly (δ Eu = 0.3–0.53) (δ Eu = Eu_N/(Sm_N × Gd_N)^{δ} 0.5).



5 Discussion

5.1 Analysis of source region and rock genesis

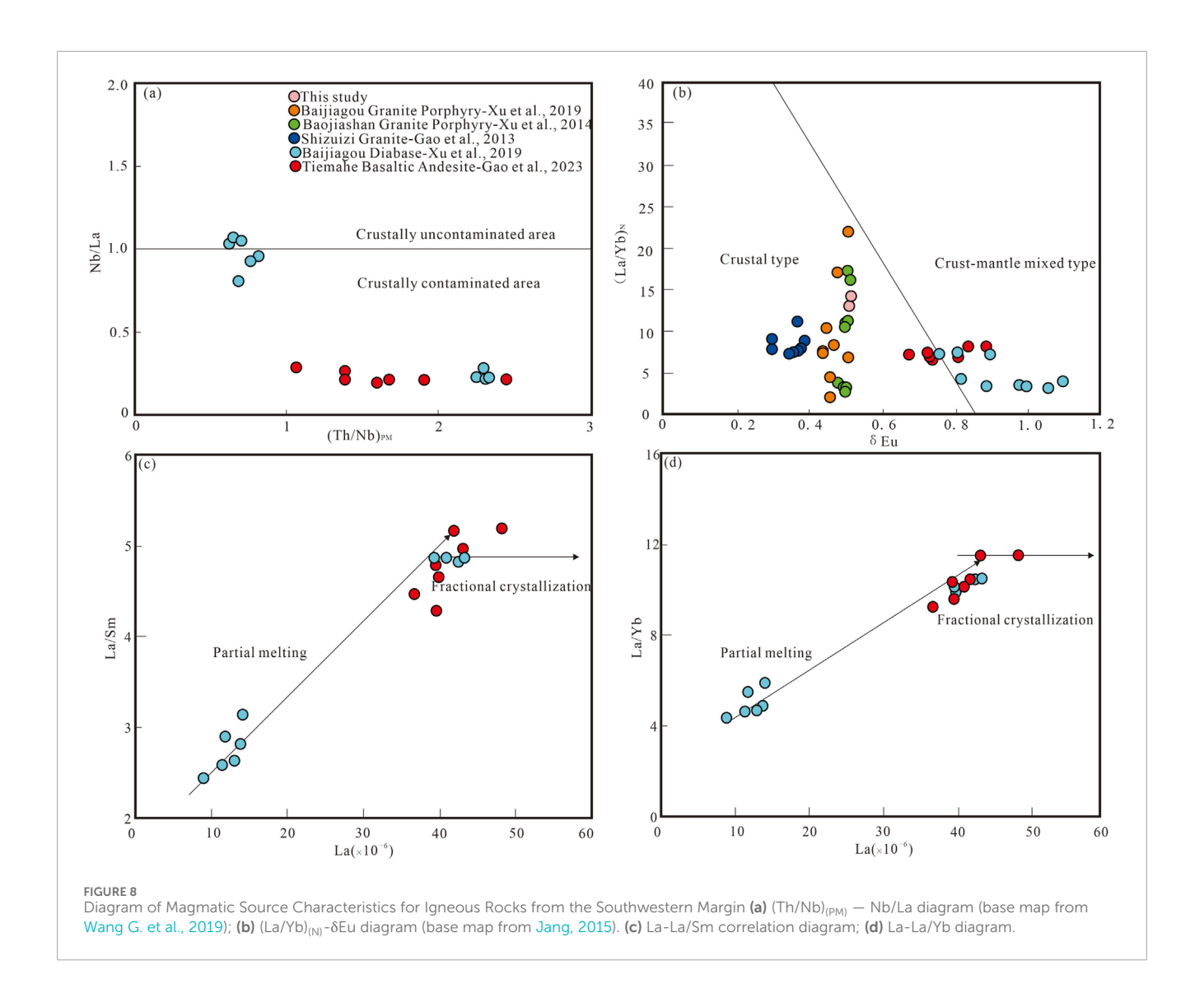
5.1.1 Analysis of granite source region and genesis

Based on the geochemical data analysis of granites in the southwestern margin of the North China Craton (Xu et al., 2014; Xu et al., 2019; Gao et al., 2013), the granite samples have relatively low contents of MgO (0.06%–1.75%, with an average of 0.69%) and CaO (0.23%–6.1%, with an average of 1.37%), while high contents of K_2O and Na_2O , reflecting alkaline characteristics. Meanwhile, they are enriched in rare earth elements, especially light rare earth elements, which is consistent with the characteristics of A-type granites (Xi et al., 2024; Liu W. et al., 2024). The granite type can be determined using the (Zr + Nb + Ce + Y)—[(K_2O + Na_2O)/CaO] diagram (Figure 8a). All granite samples from the southwestern margin fall into the A-type granite field in the discriminant diagram (Figure 7a), and plot into the A_2 -type granite field in the Nb-Y-Ce diagram (Figure 7b).

The genesis of A-type granites is relatively complex. Previous studies on the genesis of A-type granites mainly include the following viewpoints: (1) They are formed by low-degree melting of residual lower crustal granulites after the extraction of I-type granitic magma (King et al., 1997; Bonin, 2007); (2) They are formed by the melting of crustal rocks heated by underplating of mantle-derived magma (Aye et al., 2025; Faisel et al., 2025); (3) They are formed by highly fractional crystallization of mantle-derived basaltic magma (Kerr and Fryer, 1993); (4) They are formed by the mixing of crust-derived granitic magma and mantle-derived mafic magma (Yang et al., 2006; Amuda et al., 2021).

The granite samples from the southwestern margin are relatively enriched in light rare earth elements (Figure 5b). Among them, the strongly depleted Ti values and high Zr contents indicate that the source region of the granites is most likely originated from the crust, and they were formed in a tectonic setting of crustal thinning (Eby, 1992). The average Rb/Sr ratios of the mantle and crust are 0.03 and 0.35, respectively (McDonough and Sun, 1995). The average Rb/Sr ratios of the Baojiashan granite porphyry, Shizuizi granite, Baijiagou granite, and the Qian'gou granite porphyry studied in this paper are 2.69, 1.93, 1.79, and 3.25, respectively, all of which are higher than the crustal average. Therefore, the source region is more likely originated from the upper crust (Taylor and McLennan, 1985). The high La/Nb ratios (0.91-8.37) with an average of 4.19 also suggest that the magma was derived from a crustal source (Liu et al., 2024). Meanwhile, the depletion of Nb and Ta may be due to the involvement of continental crust components, and the obvious negative Eu anomaly in the chondritenormalized distribution curve of rare earth elements also reflects the characteristics of a crustal source (Pan et al., 2025). Mg# is an important parameter for determining the magma source. Generally, if mantle materials are involved in rock formation, the Mg[#] of the rock mass will be greater than 45 (Tatsumi, 2006). High-Mg andesites in the Setouchi volcanic belt, southwestern Japan: Analogues for Archean magmatism and continental crust formation? Annual Review of Earth and Planetary Sciences, 34, 467–499. The average Mg[#] values of the Baijiagou area, Shizuizi area, Baojiashan area, and the Qian'gou area studied in this paper are 20.34, 10.1, 10.92, and 29.4, respectively. These low Mg# values are also important evidence that the magma was derived from the crust (Rapp and Watson, 1995; Smithies, 2000).

The chondrite-normalized (La/Yb) ratio can indicate the degree of fractionation between light and heavy rare earth elements, while the δEu value can effectively reflect the degree of plagioclase



fractional crystallization (Jang, 2015). The (La/Yb) $_{\rm N}$ - δ Eu diagram (Figure 8b) can reveal the source material origin of igneous rocks and the continuity of magmatic evolution (Jang, 2015). It can be seen from the diagram that all granites in the southwestern margin belong to the crustal type. Combined with the above geochemical data, it can be judged that the Mesoproterozoic granites in the southwestern margin were all formed by crustal melting.

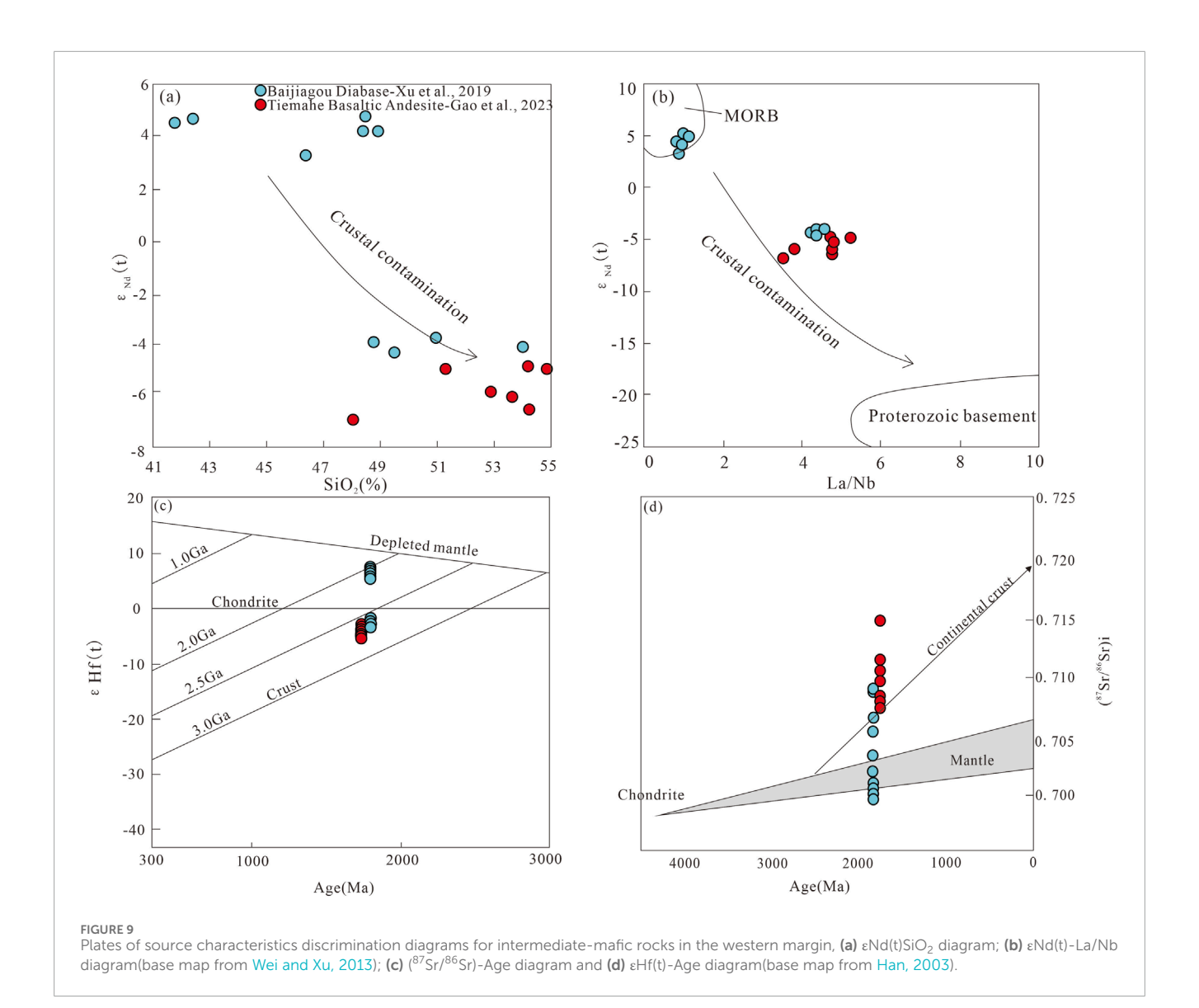
5.1.2 Analysis of source region and genesis of intermediate-mafic rocks

In addition to granites, the Mesoproterozoic igneous rock assemblages in the western margin of the North China Craton also include intermediate-mafic rocks, such as the basaltic andesites (1740 \pm 17) from the Tiemahe area and the diabase (1804 \pm 21) from the Baijiagou area (Xu et al., 2019; Gao et al., 2023). These intermediate-mafic rocks, along with the granites analyzed earlier, were formed during the early Mesoproterozoic era and in geographically proximate locations, leading to the inference that they belong to the same magmatic event. Therefore, this study examines the geochemical characteristics of these intermediate-mafic rocks to clarify the nature of their magma source and genetic

mechanisms. By integrating the aforementioned granitic rocks, a comprehensive investigation is conducted to systematically reveal the tectonic setting of the Mesoproterozoic magmatic activity in the western margin.

5.1.2.1 Fractional crystallization

The basaltic andesites from Tiemahe and diabases from Baijiagou show no obvious depletion in Zr and Hf, nor in heavy rare earth elements (HREEs) (Figures 6c,d), indicating the absence of fractional crystallization of garnet-like minerals. However, the relative depletion of Sr and negative Eu anomalies suggest fractional crystallization of plagioclase. The positive correlation between Cr, Ni, Dy, and Er in some samples indicates the fractional crystallization of ferromagnesian minerals. In the La-La/Sm diagram (Figure 8c), it can be observed that most basaltic andesites show a trend of partial melting with a certain degree of fractional crystallization. The diabases can be divided into low-Ti and high-Ti types: the low-Ti type is mainly dominated by fractional crystallization, while the high-Ti type shows a trend of partial melting (Li et al., 2019). In the La-La/Yb diagram (Figure 8d), some basaltic andesites also fall into the fractional crystallization field;



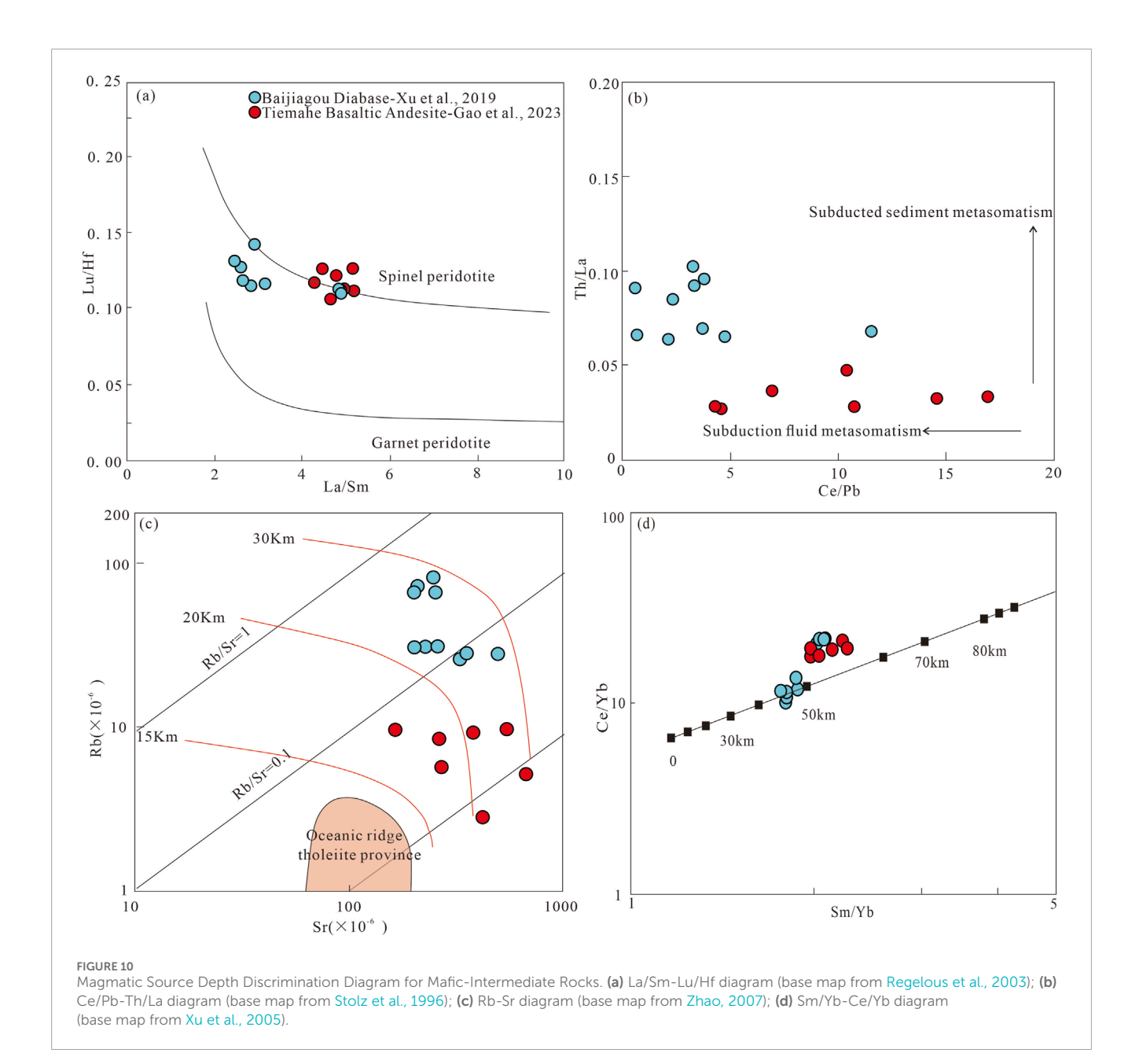
for diabases, the high-Ti type is related to partial melting, while the low-Ti type is dominated by fractional crystallization. Therefore, it can be concluded that the magma of basaltic andesites in the depletion in high field strength elements of the depletion in high field strength elements.

study area was mainly formed by partial melting with a certain degree of fractional crystallization, possibly involving the fractional crystallization of ferromagnesian minerals and plagioclase, whereas the low-Ti diabases were mainly formed by fractional crystallization.

5.1.2.2 Crustal contamination

During the ascent of magma, it may undergo crustal contamination, leading to changes in magma composition. In the $(Th/Nb)_{PM}$ -Nb/La diagram (Figure 8a), it can be observed that the sample points of basaltic andesites and low-Ti diabases all fall within the field affected by crustal contamination, while some high-Ti diabases lie in the field without crustal contamination. In the $(La/Yb)_{N}$ - δ Eu diagram (Figure 8b), both diabases and andesites are classified as crust-mantle mixed type (Jang, 2015).

In the primitive mantle-normalized trace element spider diagram, basaltic andesites and low-Ti diabases show obvious depletion in high field strength elements (HFSEs) such as Nb and Ta (Xia et al., 2011), indicating the addition of crustal materials. Meanwhile, the Sr and Nd isotopic ratios of mantle-derived magma evolve toward the crustal direction due to contamination by crustal materials. The diagrams of Nd isotopes versus SiO2 and La/Nb ratios (Figures 9a,b) can easily identify crustal contamination, from which it can be seen that basaltic andesites and low-Ti diabases are obviously affected by crustal contamination. Additionally, in the diagrams of Sr and Hf isotopes versus age (Figures 9c,d), basaltic andesites and low-Ti diabases are located in the crustal field, while high-Ti diabases lie in the mantle field. The Zr/Hf ratio is a good indicator for distinguishing magma source regions: the Zr/Hf ratio is approximately 50 in the mantle and about 36 in the crust (Anderson, 1983). This low average Zr/Hf ratio (37.35) in basaltic andesites and diabases indicates, which also indicates that the magma of basaltic andesites and low-Ti diabases has experienced crustal contamination (Zhou et al., 2024).



5.1.2.3 Source region characteristics

The La/Sm-Lu/Hf covariance system of basaltic andesite and diabase samples has clear tectonic indicative significance in the genetic discrimination diagram (Figure 10a). The data of basaltic andesites and low-Ti diabases are concentrated along the evolutionary trend line of spinel lherzolite (Regelous et al., 2003), indicating that their mantle source region is located in the spinel-facies stability domain at a depth of <80 km. In contrast, high-Ti diabases are close to the garnet peridotite field, which proves that their mantle source region may be at a depth of >80 km. Meanwhile, high-Ti diabases have not undergone plagioclase crystallization (without obvious negative Eu-Sr anomalies), and their REE distribution patterns are similar to those of other diabase types, suggesting that their source involves garnet. This also confirms that the magma source of high-Ti diabases is deeper than 80 km, possibly derived from mantle plumes or asthenospheric magma.

The average La/Nb ratio of basaltic andesites and low-Ti diabases is 4.45, which is greater than 1.50, reflecting that the magma source region has the characteristics of enriched mantle and crustal contamination. The average La/Ta ratio of basaltic andesite samples reaches 31.5, and that of low-Ti diabases is 84.2, both of which are higher than the discrimination threshold for magmas derived from the lithospheric mantle source region (La/Ta >25) (Lassiter and Depaolo, 1997). Meanwhile, the Nb/La ratios of basaltic andesites and low-Ti diabases are low (with an average of 0.22), showing a significant difference from asthenospheric mantle melts that are not contaminated by the lithosphere (Nb/La >1), whereas the average Nb/La ratio of high-Ti diabases is 1.01, which is consistent with asthenospheric mantle melts. In addition, in the Ce/Pb-Th/La diagram (Figure 10b), it can be observed that the samples of basaltic andesites and low-Ti diabases have been metasomatized by subduction fluids.

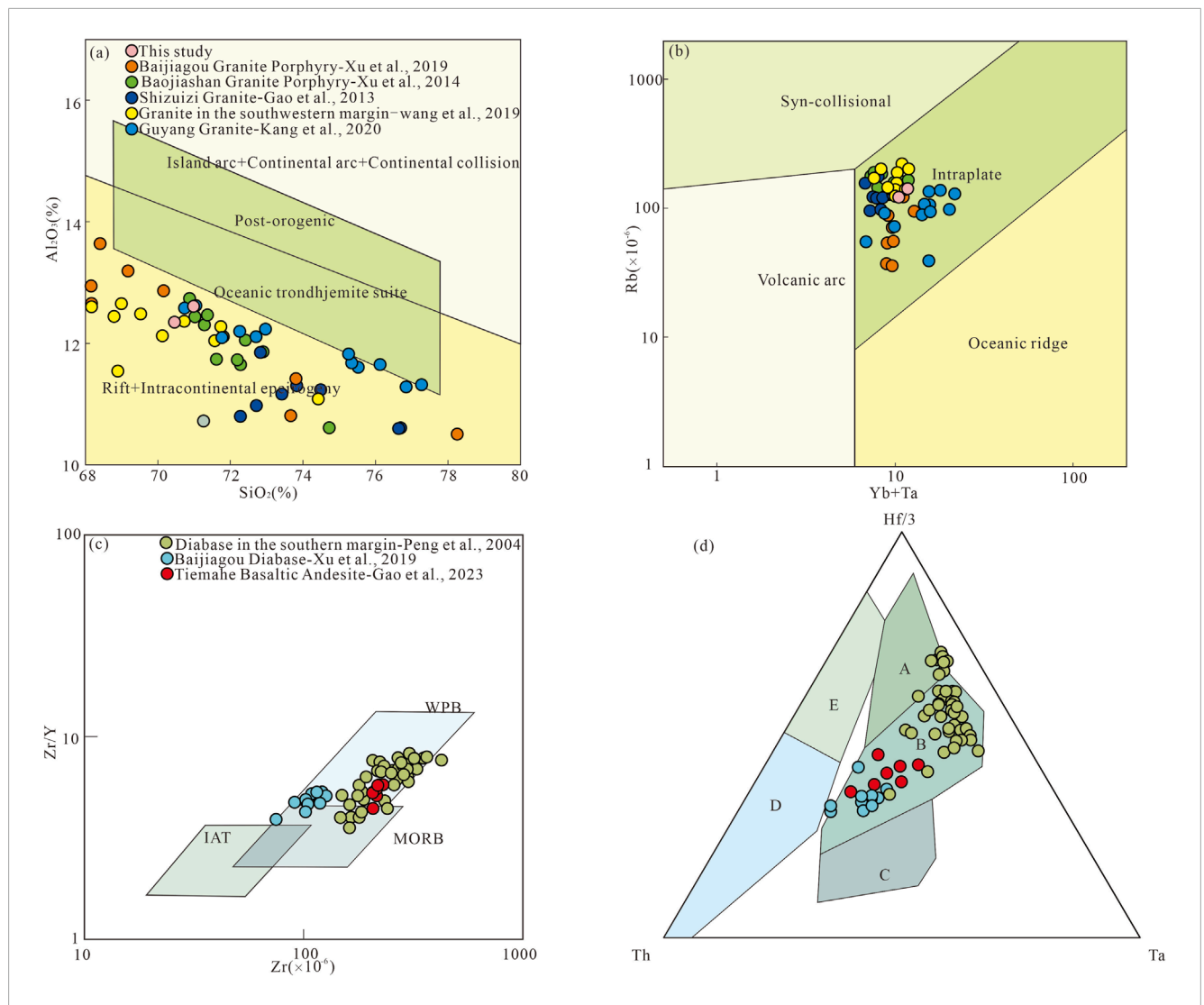


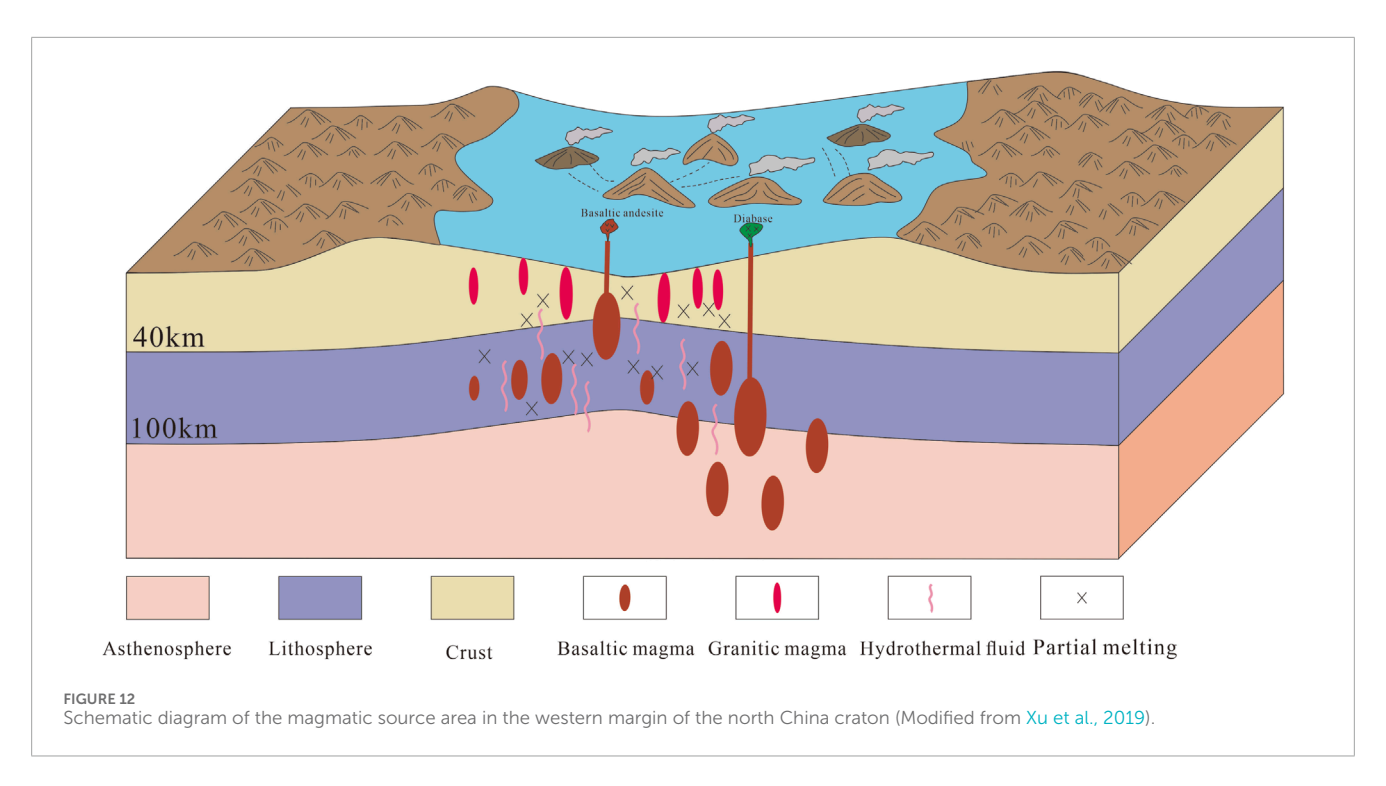
FIGURE 11 Tectonic Setting Discrimination Diagram for Igneous Rocks the southwestern margin. (a) $SiO_2-Al_2O_3$ diagram (base map from Maniar and Piccoli, 1989); (b) (Yb + Ta)-Rb diagram (base map from Pearce et al., 1984); (c) Zr-Zr/Y diagram (base map from Xia et al., 2007); (d) Zr-Zr-Y diagram (base map from Xia et al., 2007); (d) Zr-Zr-Y diagram (from Wood, 1980). Note for (c): WPB, within-plate basalt; MORB, mid-ocean ridge basalt; IAB, island arc basalt; Note for (d): A, depleted mid-ocean ridge basalt; B, enriched mid-ocean ridge basalt and within-plate basalt; C, within-plate alkaline basalt; D, calc-alkaline basalt; E, island arc basalt.

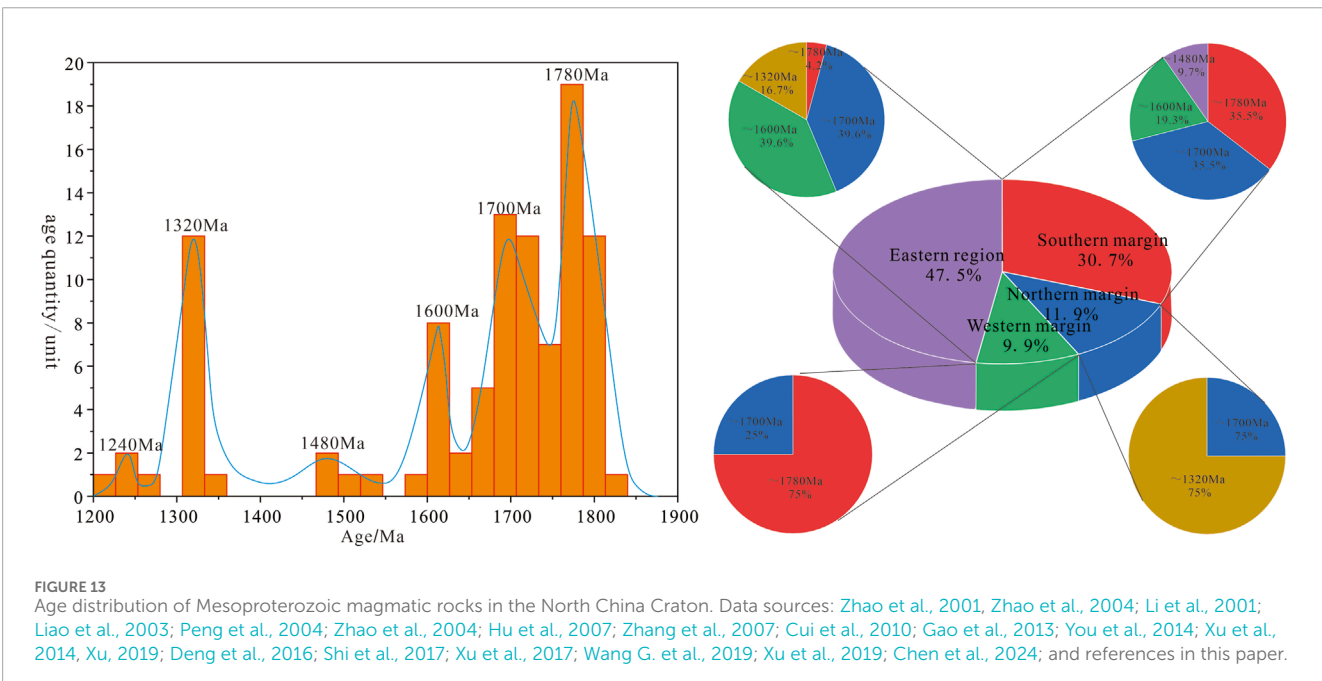
In the Sr-Rb diagram, it can be observed that the crustal thickness during the formation of basaltic andesites and diabases was 15–30 km. The Sm/Yb-Ce/Yb diagram shows that the lithospheric thickness of high-Ti diabases was 40–50 km (Figures 10c,d), whereas that of basaltic andesites and low-Ti diabases was 50–60 km. Therefore, during the late Paleoproterozoic and early Mesoproterozoic in the southwestern margin, the upwelling of mantle plumes caused lithospheric thinning, and partial melting occurred in the upper crust. The melted crustal materials formed A-type granites. In the early stage, the upwelling mantle plume materials mixed with crustal materials to form basaltic andesites and low-Ti diabases. In the late stage, as the lithosphere further thinned, the mantle plume materials directly formed diabase magma.

5.2 Regional tectonic analysis

The granite samples from the southwestern margin are A-type granites, which are known for their alkaline, anhydrous, and non-orogenic characteristics. The samples plot in the A_2 -type granite field in the A-type granite classification diagram. A_2 -type granites are post-orogenic granites, associated with mechanisms such as post-collisional extension and back-arc extension (Loiselle and Wones, 1979). In the Rb-(Yb + Ta) diagram (Figure 11a), the samples fall into the within-plate granite (WPG) tectonic setting; in the SiO_2 -Al $_2O_3$ diagram (Figure 11b), they plot in the rift-related and intracontinental epeirogenic uplift fields.

The geochemical characteristics of basaltic andesite and diabase samples show significant enrichment in light rare earth elements





(LREEs) and large ion lithophile elements (LILEs), accompanied by systematic depletion in high field strength elements (HFSEs). The Zr content is notably high (88.2–229), and the Zr/Y ratio is higher than that of island arc basalts (<4). In the Zr-Zr/Y diagram (Figure 11c), most samples fall into the within-plate basalt field; in the Hf/3-Th-Ta diagram (Figure 11d), they plot in the enriched mid-ocean ridge basalt (E-MORB) and within-plate basalt fields (Wood, 1980). Therefore, the igneous rocks in the southwestern margin should all belong to a within-plate tectonic environment. The North China Craton was in a post-orogenic extensional stage during the 1.80 Ga period. Combined with the above inference on the genesis of igneous

rocks, it is proposed that during the late Paleoproterozoic to early Mesoproterozoic, the North China Craton began to extend, and the upwelling of mantle plumes in the southwestern margin caused lithospheric thinning, leading to partial melting of the upper crust. A series of magmatic activities occurred as a result (Figure 12).

During the Mesoproterozoic, multiple magmatic activities occurred in the North China Craton, which can be roughly divided into five stages. Among them, the period of 1.80–1.77 Ga marked the initiation of Mesoproterozoic magmatic activities and represented a transitional stage when the craton shifted from a collisional orogenic environment to an extensional one (Peng et al., 2004; Xiang et al.,

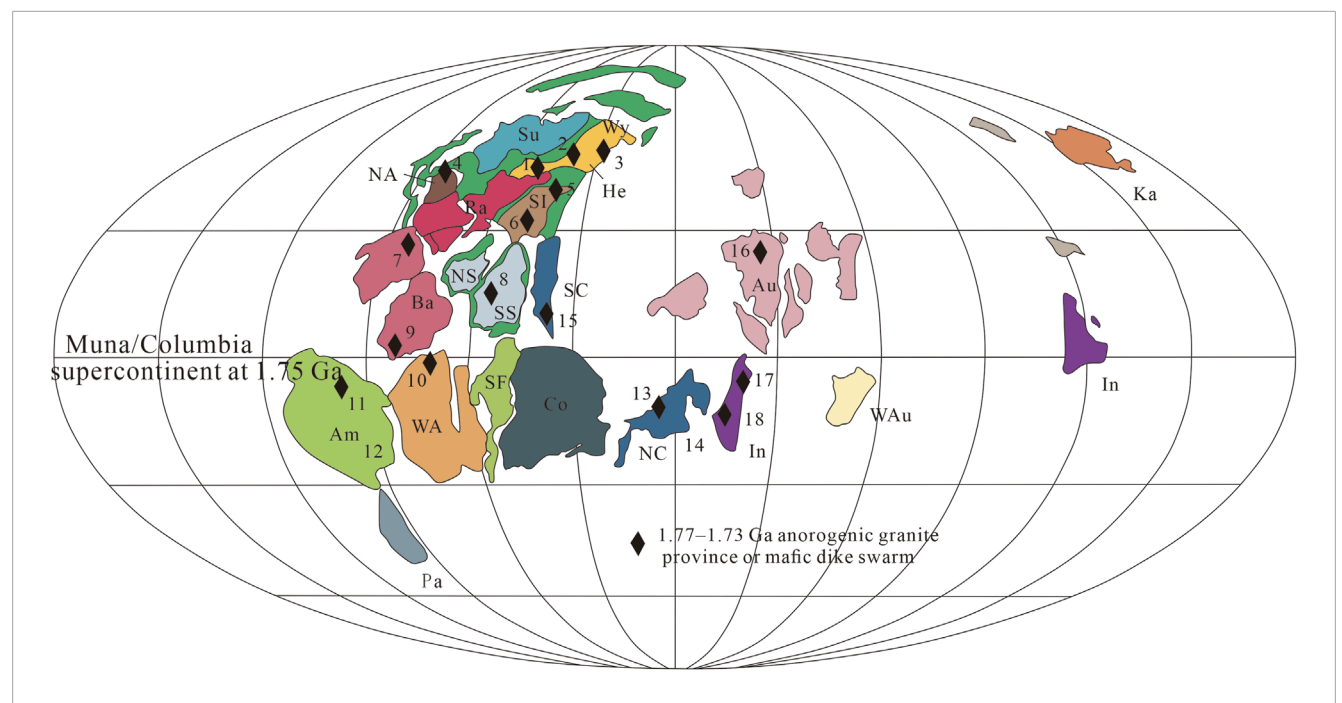


FIGURE 14
Distribution of the Nuna/Columbia supercontinent at 1750 Ma and representative 1.77–1.73 Ga anorogenic granite provinces or basic dyke swarms (modified from Peterson et al., 2015). Abbreviations for cratons or continental fragments: Am, Amazonia; Au, Australia; Ba, Baltic Shield; Co, Congo; He, Hearne; In, India; Ka, Karelia; NA, North Atlantic; NC, North China; NS, North Siberia; Ra, Rae; Pa, Proto-Australia; SC, South China; SI, Slave; SF, São Francisco; SS, South Siberia; Su, Superior; WA, West Africa; WAu, Western Australia; Wy, Wyoming.

2020). This period was typified by the Xionger Group volcanic rocks on the southern margin of the North China Craton and the basic dyke swarms in the Wutai and Hengshan areas, characterized by distinct bimodal or igneous rock features (Zhao et al., 2004; Zhao et al., 2012). In combination with the regional tectonic setting, these volcanic rocks are believed to have formed in a continental margin triple rift environment. Together with the widely distributed basic dyke swarms within the North China Craton, they are regarded as products of extensional rifting immediately following cratonization (Zhao et al., 2004; Geng et al., 2019).

The magmatic activities in the southwestern margin studied herein also took place during this period and are located on the southwestern margin of the Ordos Basin, close to the distribution area of the Xiong'er Group. Moreover, plotting of the igneous rock data from the southern margin on tectonic discrimination diagrams reveals that their tectonic setting is essentially identical to that of the southwestern margin (Figure 12). Furthermore, integrated with previous literature, it is suggested that the igneous rocks from the southern margin share a similar origin with those from the southwestern margin (Peng et al., 2004; Wang C.M. et al., 2019; Kang et al., 2020). Therefore, the magmatic activities in the southwestern margin should be an extension of the igneous activities of the Xiong'er Group, and the southwestern margin of the Ordos Basin should have been part of the triple rift system on the southern margin of the North China Craton in the early Mesoproterozoic.

As a key component of the Columbia supercontinent, controversies remain regarding the timing and dynamic mechanisms of the North China Craton's breakup (Lu et al., 2002; Zhai et al., 2014; Zhai et al., 2021; Geng et al., 2019;

Huang et al., 2020). Studies have indicated that the North China Craton experienced multiple episodes of breakup during the Mesoproterozoic: the 1.78 Ga Xiong'er Group igneous rocks and basic dykes marked the initial breakup after cratonization; subsequent magmatic activities during 1.72-1.67 Ga were concentrated in areas such as southwestern Liaoning, eastern Hebei, and Inner Mongolia on the northern margin; volcanic rocks and alkaline rocks from 1.63-1.62 Ga are found in the Yanliao Rift, the southern margin, and the southwestern Shandong region; diabase intrusions from 1.33-1.30 Ga are widely distributed in the eastern segment of the Yanliao Rift and areas such as Shangdu-Huade in the north; and the final magmatic event from 1.23-1.20 Ga marked the end of this stage (Peng et al., 2004; Hu et al., 2007; Zhai et al., 2014; Geng et al., 2019; Xiang et al., 2020) (Figure 13). These successive magmatic activities suggest that the breakup process of the North China Craton spanned the entire Mesoproterozoic, and its dynamic background should be closely related to the breakup process at the supercontinental scale.

During the stretching and breakup of supercontinents, various types of anorogenic magmatism are commonly associated. Volcanic rocks are mostly characterized by bimodal volcanic rocks, while intrusive rocks are represented by plagioclase rocks, granophyric monzonites, charnockites, granites (AMCG suites), rapakivi granites, and basic dyke swarms (Hou et al., 2008; Ernst et al., 2016; Geng et al., 2019). Large-scale anorogenic magmatic events were widespread in the Columbia supercontinent around 1.78 Ga (Figure 14). In addition to the basic dykes and anorogenic granites in the North China Craton, these include numerous 1.8–1.7 Ga anorogenic granites and basic dyke swarms exposed in the Volyn, Ingul, and Azov blocks on the northern margin of the Ukrainian Shield. The southern part of the

Siberian Craton also contains records of magmatic activities related to the early breakup of the Columbia supercontinent, including the 1.758–1.752 Ga Timpton-Algamaisky and 1.751 Ga Chaiskii basic dyke swarms (Gladkochub et al., 2010; Ernst et al., 2016). The 1.78 Ga magmatic event in the North China Craton is highly consistent with these global events in terms of spatiotemporal distribution, rock assemblages, and geochemical characteristics. Therefore, this study concludes that the North China Craton was indeed involved in the breakup process of the Columbia supercontinent, and the 1.78 Ga magmatic event should mark the initiation of the Columbia supercontinent's breakup.

Based on the above analysis, the 1.78 Ga magmatic activities in the southwestern margin of the North China Craton, as the northwestward extension of the Xiong'er Group volcanic belt, share a unified geodynamic background in terms of genetic mechanism with the triple rift system in the southern margin. This magmatic event not only represents the establishment of the post-orogenic extensional regime in the North China Craton but also constitutes the initial geological record of the global breakup process of the Columbia supercontinent within the North China Craton.

6 Conclusion

- 1. The granitoids (1781–1803 Ma) in the southwestern margin of the North China Craton belong to shoshonitic A_2 -type granites, characterized by enrichment in LILEs (Rb, Ba, K), depletion in HFSEs (Nb, Ti, P), significant negative Sr anomalies, enrichment in light rare earth elements (LREEs), flat heavy rare earth elements (HREEs), obvious negative Eu anomalies, and relatively low Mg#. Combined with other geochemical characteristics, they indicate a origin from crustal melting.
- 2. The coeval intermediate-mafic rocks (1740–1804 Ma) include calc-alkaline basaltic andesites and high-K calc-alkaline diabases. Among them, basaltic andesites and low-Ti diabases underwent fractional crystallization. The Sr and Nd isotopic ratios, Sr-Hf isotope-age diagrams, and geochemical characteristics reveal significant crustal contamination in basaltic andesites and low-Ti diabases, indicating that their genesis involved mixing between mantle plume and crustal materials, whereas high-Ti diabases were directly derived from mantle plume melting.
- 3. The Mesoproterozoic igneous rocks in the southwestern margin formed in a post-orogenic intracontinental extensional setting, representing the extension of the Xiong'er Group magmatism. Their genetic mechanism shares a unified geodynamic background with the triple rift system in the southern margin. This magmatism not only marks the establishment of the post-orogenic extensional regime in the North China Craton but also constitutes the initial geological record of the global breakup process of the Columbia supercontinent within the North China Craton.

Data availability statement

The raw data supporting the conclusions of this article will be made available by the authors, without undue reservation.

Author contributions

JC: Writing – original draft. WG: Writing – review and editing. JR: Writing – review and editing. ZR: Writing – review and editing. HS: Data curation, Writing – review and editing. GL: Software, Writing – original draft.

Funding

The author(s) declare that financial support was received for the research and/or publication of this article. PetroChina Changqing Oilfield Major Science and Technology Program (No. 2024D1JC06).

Acknowledgements

We thank the State Key Laboratory of Continental Evolution and Early Life at Northwest University for their technical assistance with our experimental data analysis. We are also grateful to Professor Hossein Azizi and the two reviewers for their insightful comments, which have significantly improved this work.

Conflict of interest

Author JR was employed by Exploration and Development Research Institute of PetroChina Changqing Oilfield Company.

The remaining authors declare that the research was conducted in the absence of any commercial or financial relationships that could be construed as a potential conflict of interest.

The authors declare that this study received funding from the PetroChina Changqing Oilfield Major Science and Technology Program. The funder was involved in the following aspects of the study: data collection and analysis.

Generative AI statement

The author(s) declare that no Generative AI was used in the creation of this manuscript.

Any alternative text (alt text) provided alongside figures in this article has been generated by Frontiers with the support of artificial intelligence and reasonable efforts have been made to ensure accuracy, including review by the authors wherever possible. If you identify any issues, please contact us.

Publisher's note

All claims expressed in this article are solely those of the authors and do not necessarily represent those of

their affiliated organizations, or those of the publisher, the editors and the reviewers. Any product that may be evaluated in this article, or claim that may be made by its manufacturer, is not guaranteed or endorsed by the publisher.

References

- Amuda, A. K., Yang, X., Deng, J., Faisal, M., Cao, J., Bute, S. I., et al. (2021). Petrogenesis of the peralkaline Dutsen Wai and Ropp complexes in the Nigerian younger granites: implications for crucial metal enrichments. *Int. Geol. Rev.* 63 (16), 2057–2081. doi:10.1080/00206814.2020.1821250
- Anderson, J. L. (1983). Proterozoic anorogenic granite pluto-nism of North America. *Geol. Soc. Am.* 161, 133–154. doi:10.1130/MEM161-p133
- Aye, P. P., Li, H., Hu, X. J., Majid, G., Aung, Z. M., and Mohamed, F. (2025). Geology, geochemistry, and zircon U-Pb geochronology of the Nanthila and Pedet granites in the Myeik Sn-W district, Tanintharyi region, southern Myanmar. *Ore Geol. Rev.* 178, 0169–1368. doi:10.1016/j.oregeorev.2025.106488
- Black, L. P., Kamo, S. L., Allen, C. M., Aleinikoff, J. N., Davis, D. W., Korsch, R. J., et al. (2003). Temora 1: a new zircon standard for phanerozoic u-pb geochronology. *Chem. Geol.* 200 (1), 155–170. doi:10.1016/S0009-2541(03)00165-7
- Bonin, B. (2007). A-type granites and related rocks: evolution of a concept, problems and prospects. *Lithos* 97 (1/2), 1–29. doi:10.1016/j.lithos.2006.12.007
- Chen, J., Yang, M. H., Jia, H. C., Zhang, W., Liu, X., Gang, T., et al. (2024). Petrogenesis and tectonic significance of Mesoproterozoic A-Type granites in the north China craton. *Chin. J. Geol.* 59 (01), 1–20. doi:10.12017/dzkx.2024.001
- Cui, M. L., Zhang, B. L., Peng, P., Zhang, L. C., Shen, X. L., Guo, Z. H., et al. (2010). Zircon/xenotime U-Pb dating of early Proterozoic intermediate-acid intrusive rocks in the Xiaoshan area, western Henan, and its constraints on the timing of the Xiong'er volcanic rock series. *Acta Petrol. Sin.* 26 (05), 1541–1549.
- Deng, X. Q., Peng, T. P., and Zhao, T. P. (2016). Geochronology and geochemistry of the Late Paleoproterozoic aluminous A-type granite in the Xiaoqinling area along the southern margin of the North China craton:petrogenesis and tectonic implications. *Precambrian Res.* 285, 127–146. doi:10.1016/j.precamres.2016.09.013
- Eby, N. G. (1992). Chemical subdivision of the a-type gran-itoids: petrogenetic and tectonic implications. *Geology* 20 (7), 641–644. doi:10.1130/0091-7613(1992)020<0641:csotat>2.3.co;2
- Ernst, R. E., Hamilton, M. A., Soderlund, U., Hanes, J. A., Gladkochub, D. P., Okrugin, A. V., et al. (2016). Long-lived connection between southern Siberia and northernLaurentia in the Proterozoic. *Nat. Geosci.*, 9, 464–469. doi:10.1038/NGEO2700
- Faisal, M., Yang, X. Y., Khalifa, I. H., Amuda, A. K., and Sun, C. (2020). Geochronology and geochemistry of Neoproterozoic Hamamid metavolcanics hosting largest volcanogenic massive sulfide deposits in eastern desert of Egypt: implications for petrogenesis and tectonic evolution. *Precambrian Res.* 344, 105751. doi:10.1016/j.precamres.2020.105751
- Faisal, M., Li, H., Sun, C., Muhammad, A. G., Abdulgafar, K. A., Sun, W. B., et al. (2025). Geodynamic record of Rodinia breakup to Gondwana formation: insights from bulk geochemistry, whole-rock Sr-Nd isotopes, and zircon U-Pb-Hf data of Katherina ring complex, Sinai Peninsula, Egypt. *Geosci. Front.* 16 (4), 102082. doi:10.1016/j.gsf.2025.102082
- Gao, S. L., Lin, J. Y., and Lu, Y. J. (2013). Formation epoch and its geological implications of Paleoprotozoic A-ype granite in Shizuizi of Jingyuan County, Ningxia Province. *Acta Petrol. Sin.* 29 (8), 2676–2684.
- Gao, S. L., Liu, S. L., and Zhang, Z. B. (2023). Geochemical characteristics and tectonic implications of mesoproterozoic basaltic andesites from the southwestern margin of the ordos block. *Geol. Rev.* 69 (01), 164–178. doi:10.16509/j.georeview.2022.08.02
- Geng, Y. S., Kuang, H. W., Du, L. L., Liu, Y. Q., and Zhao, T. P. (2019). On the Paleo-Mesoproterozoic boundary from the breakup event of the Columbia supercontinent. *Acta Petrol. Sin.* 35 (08), 2299–2324. doi:10.18654/1000-0569/2019.08.02
- Gladkochub, D. P., Pisarevsky, S. V., Ernst, R., Donskaya, T. V., Sderlund, U., Mazukabzov, A. M., et al. (2010). Large igneous province of about 1750Ma in the Siberian Craton. *Dokl. Earth Sci.* 430, 168–171. doi:10.1134/S1028334X10020042
- Han, Y. W. (2003). Geochemistry. Beijing: Geological Publishing House, 224–228.
- He, D. F. (2022). Multi-cycle superimposed sedimentary basins in China: Formation, evolution, geologic frame work and hydrocarbon occurrence. *Earth Sci. Front.* 29 (6), 024–059. doi:10.13745/j.esf.sf.2022.8.1
- Hou, G. T., Santosh, M., Qian, X. L., Lister, G., and Li, J. H. (2008). Configuration of the late Paleoproterozoic supercontinent Columbia: insights from radiating mafic dyke swarms. *Gondwana Res.* 14 (3), 395–409. doi:10.1016/j.gr.2008.01.010

Supplementary material

The Supplementary Material for this article can be found online at: https://www.frontiersin.org/articles/10.3389/feart.2025.1664716/full#supplementary-material

- Hu, J. L., Zhao, T. P., Chen, W., and Peng, P. (2007). Characteristics and research progress of the 1.75 Ga basic dyke swarms in the north China craton. *Geotect. Metallogenia* (04), 457–470. doi:10.16539/j.ddgzyckx.2007.04.005
- Huang, B., Kusky, T. M., Johnson, T. E., Wilde, S. A., Fu, D., Polat, A., et al. (2020). Paired metamorphism in the neoarchean: a record of accretionary-to-collisional orogenesis in the north China craton. *Earth Planet. Sci. Lett.* 543, 116355. doi:10.1016/j.epsl.2020.116355
- Jang, S. H. (2015). Geochronological, petrographic, and geochemical constraints on the early paleoproterozoic igneous rocks from song county, southern margin of the North China Craton. Beijing: China University of Geosciences.
- Jiang, L. Y., Qian, M. H., He, F. Q., Qi, R., and Yin, C. (2024). Characteristics and main controlling factors of Chang7 shale oil in Triassic Yanchang Formation, Fuxian area, ordos Basin. *Pet. Geology& Exp.* 46 (5), 941–953. doi:10.11781/sysydz202405941
- Kang, J. L., Wang, H. C., Ren, Y. W., Xiao, Z. B., Xiang, Z. Q., and Zeng, L. (2020). The Baiyunchanghe A-type granites in Guyangarea, Inner Mongolia: age, geochemistry,hf isotope and response to the breakup of Columbia supercontinent. *ActaPetrologica Sin.* 36 (8), 2431–2446. doi:10.18654/1000-0569/2020.08.10
- Kerr, A., and Fryer, B. J. (1993). Nd isotope evidence for crust—mantleinteraction in the generation of A-type granitoid suites in Labrador, Canada. *Chem. Geol.* 104, 39–60. doi:10.1016/0009-2541(93)90141-5
- King, P. L., White, A. J. R., Chappell, B. W., and Allen, C. M. (1997). Characterization and origin of aluminous a-type granites from the lachlan fold belt, southeastern Australia. *J. Petrology* 38, 371–391. doi:10.1093/petroj/38.3.371
- Lassiter, J. C., and Depaolo, D. J. (1997). Plume/Lithosphere interaction in the generation of Continental and Oceanic flood basalts: Chemical and isotopic constraints. *Geophys. Monogr.* 1997, 335–355. doi:10.1029/GM100p0335
- Li, J. H., Hou, G. T., Qian, X. L., Halls, H. C., and Davis, D. (2001). Single-zircon U-Pb ages of the early Mesoproterozoic basic dyke swarms in the Hengshan Mountains and their significance for cratonic tectonic evolution. *Geol. Rev.* (03), 234–238. doi:10.16509/j.georeview.2001.03.003
- Li, W., Dong, Y., Guo, A., Liu, X., and Zhou, D. (2013). Chronology and tectonic significance of cenozoic faults in the liupanshan arcuate tectonic belt at the northeastern margin of the Qinghai–Tibet plateau. *J. Asian Earth Sci.* 73 (sep.5), 103–113. doi:10.1016/j.jseaes.2013.04.026
- Li, Z., Lang, X. H., Zhang, Q. Z., and He, L. (2019). Petrogenesis and geodynamic settings of the intermediate-acid intrusions related to the Pusangguo copper-dominated polymetallic deposit in Tibet: constraints from geochronology, geochemistry and Sr-Nd-Pb-Hf isotopes. *Acta Petrol. Sin.* 35 (03), 737–759. doi:10.18654/1000-0569/2019.03.00
- Li, Q. G., Huang, X., Chu, H., Sun, D., and Liu, W. Y. (2024). Zircon geochronology and geological implications of the Wutai greenstone belt, North China Craton. *Acta Petrol. Sin.* 40 (11), 3426–3447. doi:10.18654/1000-0569/2024.11.06
- Liao, C. L., Wang, Y. J., and Peng, T. P. (2003). \(^{40}Ar^{-39}Ar\) geochronology of Early Paleoproterozoic mafic dikes in the southern Taihang Mountains and its tectonic implications. \(\textit{Geotect.}\) \(\textit{Metallogenia}\) \(27\) (4), \(354-361\). \(\dot{doi:}10.16539/j\).ddgzyckx.2003.04.006
- Lin, J., Zhen, Q., Wang, Q., Guo, Y., Wu, C., Wu, Z., et al. (2016). Joint development and tectonic stress field evolution in the southeastern Mesozoic Ordos Basin, west part of North China. *Asian Earth Sci.* 127, 47–62. doi:10.1016/j.jseaes.2016.06.017
- Liu, G. Q., Su, Z. T., Hao, Z. L., Wei, L. B., Ren, J. F., Liao, H. H., et al. (2024). Sedimentary microfacies and sedimentary models of the carbonate-gypsum salt rock symbiotic system in the Majiagou Formation, Ordos Basin. *J. Palaeogeogr.* 26 (02), 279–295. doi:10.7605/gdlxb.2024.02.021
- Liu, W., Zhang, H. R., Luo, D. K., Jia, P. F., Jin, L. J., Zhou, Y. G., et al. (2024). Petrogenesis of Paleoproterozoic granites in the Dondo area, northern Angola Block: a response to the assembly of the Columbia supercontinent. *Earth Sci. Front.* 31 (04), 237–257. doi:10.13745/j.esf.sf.2024.2.15
- Liu, J. H., Li, Y. S., Xu, W. N., and Ding, Z. J. (2025). Formation and dynamic evolution of the Paleoproterozoic Jiao-Liao-Ji tectonic belt in the North China Craton. *Acta Geol. Sin.* 99 (01), 23–43. doi:10.19762/j.cnki.dizhixuebao.2024535
- Loiselle, M. C., and Wones, D. R. (1979). Characteristics and origin of anorogenic granites. *Geol. Soc. Am. Abstr. Programs* 11 (7), 468.

- Lu, S. N., Yang, C. L., Li, H. K., and Chen, Z. H. (2002). The North China paleocontinent and the Columbia supercontinent. *Earth Sci. Front.* (04), 225–233. doi:10.3321/j.issn:1005-2321.2002.04.002
- Luo, L. Y., Li, Y., He, Q. B., Li, S. X., and Li, X. (2024). *In-situ* gas-bearing evaluation of marine-continental transitionalshale in the eastern margin of ordos Basin and its geological application. *Nat. GasGeoscience* 35 (12), 2215–2227. doi:10.11764/j.issn.1672-1926.2024.06.002
- Maniar, P. D., and Piccoli, P. M. (1989). Tectonic discrimination of granitoids. *GSA Bull.* 101, 635–643. doi:10.1130/0016-7606(1989)101<0635:TDOG>2.3.CO;2
- McDonough, W. F., and Sun, S. S. (1995). The composition of the Earth. *Chem. Geol.* 120 (3-4), 223–253. doi:10.1016/0009-2541(94)00140-4
- Middlemost, E. A. K. (1994). Naming materials in the magma/igneous rock system. *Earth-Science Rev.* 37 (3/4), 215–224. doi:10.1016/0012-8252(94)90029-9
- Pan, S. J., Zhang, J. F., Chen, X. Y., Ma, J. X., Cai, X. L., and Huang, G. C. (2025). Formation age and genesis of syenogranites in Shengsi, Zhejiang: evidence from zircon U-Pb geochronology, petrogeochemistry, and Hf isotopes. *Earth Sci. Front.* 32 (02), 430–444. doi:10.13745/j.esf.sf.2024.11.5
- Pearce, J. A., Harris, N. B. W., and Tindle, A. G. (1984). Trace element discrimination diagrams for the tectonic interpretation of Granitic rocks. J. Petrology 25 (4), 956–983. doi:10.1093/petrology/25.4.956
- Peng, P., Zhai, M. G., Zhang, H. F., Zhao, T. P., and Ni, Z. Y. (2004). Geochemical characteristics and geological significance of the 1.8 Ga mafic dyke swarms in the north China Craton: a case study of the Shanxi-Hebei-Inner Mongolia border area. *Acta Petrol. Sin.* (03), 439–456.
- Peterson, T. D., Scott, J. M. J., LeCheminant, A. N., Jefferson, C. W., and Pehrsson, S. J. (2015). The Kivalliq igneous Suite:Anorogenic bimodal magmatism at 1.75Ga in the western Churchill Province, Canada. *Precambrian Res.* 262, 101–119. doi:10.1016/J.PRECAMRES.2015.02.019
- Rapp, R. P., and Watson, E. B. (1995). Dehydration melting of metabasalt at 8-32 kbar: implications for continental growth and crust-mantle recycling. *J. Petrology* 36 (4), 891–931. doi:10.1093/petrology/36.4.891
- Regelous, M., Hofmann, A. W., Abouchami, W., and Galer, J. G. S. (2003). Geochemistry of lavas from the emperor seamounts, and the geochemical evolution of Hawaiian magmatism from 85 to 42 Ma. *J. Petrology* 44 (1), 113–140. doi:10.1093/petrology/44.1.113
- Santosh, M. (2010). Assembling North China Craton within the Columbia supercontin-ent: the role of double-sided subduction. *Precambrian Res.* 178, 149–167. doi:10.1016/j.precamres.2010.02.003
- Santosh, M., Liu, D. Y., Shi, Y. R., and Liu, S. J. (2011). Paleoproterozoic accretionary orogenesis in the North China Craton: a SHRIMP zircon study. *Precambrian Res.* 227, 29–54. doi:10.1016/j.precamres.2011.11.004
 - Shand, S. J. (1943). The eruptive rocks. 2nd edition. New York: John Wiley, 444.
- Shi, J. P., Yang, D. B., Huo, T. F., Yang, H. T., Xu, W. L., and Wang, F. (2017). Geochronology and Nd-Hf isotopic compositions of A-type granites in the southern margin of the North China Craton: constraints on the late Paleoproterozoic extensional event. *Acta Petrol. Sin.* 33 (10), 3042–3056.
- Smithies, R. H. (2000). The Archaean tonalite–trondhjemite–granodiorite (TTG) series is not an analogue of Cenozoic adakite. *Earthand Planet. Sci. Lett.* 182 (1), 115–125. doi:10.1016/S0012-821X(00)00236-3
- Song, B., Zhang, Y. H., and Wan, Y. S. (2002). Mount making, age determination and discussion on related phenomena of zircon SHRIMP samples. *Geol. Rev.* 48 (S1), 26–30. doi:10.16509/j.georeview.2002.s1.007
- Stolz, A. J., Jochum, K. P., Spettel, B., and Hofmann, A. W. (1996). Fluid- and melt-related enrichment in the subarc mantle: evidence from Nb/Ta variations in island-arc basalts. Geol.~24~(7),~587-590.~doi:10.1130/0091-7613(1996)024<0587:FAMREI>2.3.CO;2
- Sun, J., and Dong, Y. (2019). Middle-late triassic sedimentation in the helanshan tectonic belt: constrain on the tectono-sedimentary evolution of the Ordos Basin, north China. *Geosci. Front.* 10, 213–227. doi:10.1016/j.gsf.2018.05.017
- Sun, S. S., and McDonough, W. F. (1989). Chemical and isotopic systematics of oceanic basalts: implications for mantle composition and processes. *Geol. Soc. Lond. Special Publ.* 42(1), 313–345. doi:10.1144/GSL.SP.1989.042.01.19
- Tao, H., Cui, J. P., Sun, J. P., Ren, Z. L., Zhao, F. F., Su, S. S., et al. (2025). Late carboniferous to permian paleoclimatic and tectono-sedimentary evolution of the central ordos basin, western north china block. *Mar. Petroleum Geol.* 173, 107287. doi:10.1016/j.marpetgeo.2025.107287
- Tatsumi, Y. (2006). High-Mg andesites in the Setouchi volcanic belt, southwestern Japan: analogues for Archean magmatism and continental crust formation? *Annu. Rev. Earth Planet. Sci.* 34, 467–499. doi:10.1146/annurev.earth.34.031405.125014
- Taylor, S. R., and McLennan, S. M. (1985). *The Continental crust: its composition and evolution*. Oxford: Blackwell Scientific Publications, 57–72.
- Vavra, G., Gebauer, D., Schmid, R., and Compston, W. (1996). Multiple zircon growth and recrystallization during polyphase late carboniferous to triassic metamorphism in granulites of the ivrea zone (southern alps): an ion microprobe (shrimp) study. *Contrib. Mineral. Petrol.* 122 (4), 337–358. doi:10.1007/s004100050132

- Wang, C. M., He, X. Y., Carranza, E. J. M., and Carranza, C. C. M. (2019). Paleoproterozoic volcanic rocks in the southern margin of the North China Craton, central China: implications for the Columbia supercontinent. *Geosci. Front.* 10 (4), 1543–1560. doi:10.1016/j.gsf.2018.10.007
- Wang, G., Zhang, H., Wang, Z. Q., Wu, Y. D., Wang, D. S., and Wang, J. W. (2019). Identification and tectonic significance of Permian E-MORB-type basalts in the Shiyan area of the Wudang Mountains. *Geol. Rev.* 65 (01), 65–84. doi:10.16509/j.georeview.2019.01.006
- Wei, X., and Xu, Y. (2013). Petrogenesis of the mafic dykes from Bachu and implications for the magma evolution of the Tarim large igneous province, NW China. *Acta Petrol. Sin.* 29, 3323–3335.
- Whalen, J. B., Currie, K. L., and Chappell, B. W. (1987). A-typegranites: geochemical characteristics, discrimination and petrogenesis. *Contributions Mineralogy Petrology* 95 (4), 407–419. doi:10.1007/BF00402202
- Winchester, J. A., and Floyd, P. A. (1977). Geochemical discrimination of different magma series and their differentiation products using immobile elements. *Chem. Geol.* 20, 325–343. doi:10.1016/0009-2541(77)90057-2
- Wood, D. A. (1980). The application of a th-hf-ta diagram to problems of tectonomagmatic classification and to establishing the nature of crustal contamination of basaltic lavas of the British Tertiary Volcanic Province. *Earth Planet. Sci. Lett.* 50 (1), 11–30. doi:10.1016/0012-821X(80)90116-8
- Wu, C. H., and Zhong, C. T. (1998). The Paleoproterozoic SW–NE collision model for the ce-ntral North China Craton. *Prog. Precambrian Res.* 21, 28–50.
- Xi, Z., Liu, Q. Q., Wu, D. H., and Chen, Z. H. (2024). Geochronology, geochemistry and tectonic significance of the Triassic A-type granites in the Pingtian area, northern Guangdong. *Earth Sci.* 49 (07), 2508–2525. doi:10.3799/dqkx.2023.010
- Xia, L. Q., Xia, Z. C., Xu, X. Y., Li, X. M., and Ma, Z. P. (2007). Discrimination of continental basalts and island arc basalts using geochemical methods. *Acta Petrologica Mineralogica* (01), 77–89. doi:10.3969/j.issn.1000-6524.2007.01.011
- Xia, H., Chen, G. W., Liu, Q., and Luo, Y. (2011). Geochemical characteristics and tectonic significance of volcanic rocks from the dahalajunshan Formation in the tulasu Basin, Western tianshan Mountains. *Geotect. Metallogenia* 35 (3), 429–438. doi:10.16539/j.ddgzyckx.2011.03.013
- Xiang, Z. Q. (2014). Mesoproterozoic magmatic events and metallogenesis of the north China craton. Beijing: China University of Geosciences.
- Xiang, Z. Q., Lu, S. N., Li, H. K., Tian, H., Liu, H., and Zhang, K. (2020). Mesoproterozoic magmatic event groups in the North China Craton. *Geol. Surv. Res.* 43 (02), 137–152. doi:10.3969/j.issn.1672-4135.2020.02.008
- Xu, H. (2019). Tectonic magmatic activity in the middle to late Archean of the Southwestern ordos block. Xi'an: Northwestern University.
- Xu, Y. G., Ma, J. L., Frey, F. A., Feigenson, M. D., and Liu, J. F. (2005). Role of lithosphere-asthenosphere interaction in the genesis of Quaternary alkali and tholeitic basaltsfrom Datong, western North China Craton. *Chem. Geol.* 224, 247–271. doi:10.1016/j.chemgeo.2005.08.004
- Xu, H., Zhao, H., Luo, J. H., Cheng, J. X., You, J., and Wang, S. D. (2014). Study on the Paleoproterozoic granites in Baojiashan, Longxian County, southwestern margin of the North China Block and their tectonic significance. *Geol. Rev.* 60 (06), 1284–1296. doi:10.16509/j.georeview.2014.06.007
- Xu, H., Luo, J. H., You, J., Li, Y. F., and Chen, G. C. (2017). Coeval granitic magmatism in the southern segment of the liupanshan at the sw margin of the ncc: implications for paleoproterozoic extension. *Terr. Atmos. Ocean. Sci.* 28, 877–890. doi:10.3319/TAO.2017.03.14.01
- Xu, H., Luo, J. H., Chen, G. X., You, J., and Li, Y. F. (2019). Geochronology, geochemistry and tectonic significance of a Paleoproterozoic diabase at southwestern margin of the NCC. *Terr. Atmos. Ocean. Sci.* 6 (30), 771–791. doi:10.3319/TAO.2019.05.27.02
- Yang, C. J., and Wang, Y. C. (2010). "Zircon U-Pb dating of Mesozoic granites in the Yichun area, Southeastern Xiaoxing'anling and its geological implications," 29. Jilin Geology, 1–5+31.
- Yang, H., Zhang, J., Wang, F. Y., and Wang, H. C. (2000). Characteristics of the Paleozoic gas-bearing system in the Ordos Basin. *Nat. Gas. Ind.* (06), 7–9. doi:10.3321/j.issn:1000-0976.2000.06.002
- Yang, J. H., Wu, F. Y., Chung, S. L., Wilde, S. A., and Chu, M. F. (2006). A hybrid origin for the qianshan a-type granite, northeast China: geochemical and sr nd hf isotopic evidence. *Lithos* 89, 89–106. doi:10.1016/j.lithos.2005.10.002
- Yao, Z. H., Dong, X. P., and Yang, Y. (2025). Stratigraphic Architecture and activity characteristics of the alluvial fan on the Eastern foot of Liupan Mountain since the late Pleistocene. *Geophys. Geochem. Explor.* 49 (1), 1–13. doi:10.11720/wtyht. 2025.2357
- You, J., Luo, J. H., Cheng, J. X., Wang, S. D., Xu, H., and Zhao, H. (2014). Paleoproterozoic granitic porphyries in the southwestern margin of the North China Block and their tectonic significance. *Geol. J. China Univ.* 20 (03), 368–377. doi:10.16108/j.issn1006-7493.2014.03.020
- Yuan, H. L., Wu, F. Y., Gao, S., Liu, X. M., Xu, P., and Sun, D. Y. (2003). Zircon laser probe U-Pb dating and rare earth element composition analysis of Cenozoic

intrusions in Northeast China. Chin. Sci. Bull. 14, 1511–1520. doi:10.3321/j.issn:0023-074X.2003.14.008

Zhai, M. G. (2004). 2.1-1.7Ga geological event group and geotectonie significance. Acta Petrol. Sin. 20 (6), 1343–1354. doi:10.3969/j.issn.1000-0569.2004.06.004

Zhai, M. G., and Peng, P. (2007). Paleoproterozoic events in North China Craton. *Acta-Petrologica Sin.* 23, 2665–2682. doi:10.18654/1000-0569/2021.02.04

Zhai, M. G., and Santosh, M. (2011). The early Precambrian odyssey of North China Craton: asynoptic overview. *Gondwana Res.* 24 (2), 6–12. doi:10.1016/j.gr.2011.02.005

Zhai, M. G., Guo, J. H., and Liu, W. J. (2005). Neoarchean to Paleoproterozoic continental evolution and tectonic history of the North China Craton: a review. *J. Asian Earth Sci.* 24, 547–561. doi:10.1016/j.jseaes.2004.01.018

Zhai, M. G., Hu, B., Peng, P., and Zhao, T. P. (2014). Meso-Neoproterozoic magmatism and multi-stage rifting events in North China. *Earth Sci. Front.* 21 (01), 100–119

Zhai, M. G., Zhang, Y. B., Li, Q. L., Zou, Y., He, H. L., Shan, H. X., et al. (2021). Cratons, lower crust and continental lithosphere: in celebration of the centenary of mr. Shen Qihan. *Acta Petrol. Sin.* 37 (01), 1–23. doi:10.18654/1000-0569/2021.01.01

Zhang, Y. Q., Liao, C. Z., Shi, W., and Hu, B. (2006). Neotectonic evolution and regional geodynamic setting of the peripheral zones of the ordos Basin. *J. China Univ. Geosciences* (03), 285–297.

Zhang, S. H., Liu, S. W., Zhao, Y. S., Yang, J. H., Song, B., and Liu, X. M. (2007). The 1.75-1.68 Ga anorthosite-mangerite-alkali granitoid-rapakivi granite suite from the northern North China Craton: magmatism related to a Paleoproterozoic orogen. *Precambrian Res.* 155 (3-4), 287–312. doi:10.1016/j.precamres.2007.02.008

Zhao, H. G. (2007). Study on metallogenic model of Mesozoic epithermal Cu-Au deposits in Yanbian. Jilin: Jilin University.

Zhao, G. C., and Zhai, M. G. (2013). Lithotectonic elements of Precambrian basement in the North China Craton: review and tectonic implications. *Gondwana Res.* 23 (4), 1207–1240. doi:10.1016/j.gr.2012.08.016

Zhao, T. P., Zhou, M. F., Jin, C. W., Guan, H., and Li, H. M. (2001). Discussion on the formation age of the Xionger Group in the southern margin of the North China block. *Chin. J. Geol.* (03), 326–334. doi:10.3321/j.issn:0563-5020. 2001.03.007

Zhao, T. P., Zhai, M. G., Xia, B., Li, H. M., Zhang, Y. X., and Wan, Y. S. (2004). SHRIMP zircon geochronology of the Xiongèr Group volcanic rocks: constraints on the initial tim e of cover development in the North China Craton. *Chin. Sci. Bull.* (22), 2342–2349. doi:10.3321/j.issn:0023-074X.

Zhao, G., Cawood, P. A., Li, S., Wilde, S. A., Sun, M., Zhang, J., et al. (2012). Amalgamation of the north china craton: key issues and discussion. *Precambrian Res.* 222-223 (12), 55–76. doi:10.1016/j.precamres.2012.09.016

Zhao, F. F., Cui, J. P., Ren, Z. L., Tao, H., Jiang, A. D., Su, S. H., et al. (2025). Analysis of the hydrocarbon - charging stages of the Permian in the central Ordos Basin: a case study of the Shanxi and Shihezi Formations in Wuqi area, Shaanxi. *Geol. Bull. China* 44 (05), 778–791. doi:10.12097/gbc.2024.10.011

Zhou, F. S., Lin, X., Wang, Z. R., and Shao, C. B. (2024). Genesis and significance of basaltic andesites in the Shaowu area, northern Fujian: constraints from geochronology, geochemistry, and Nd-Hf isotopes. *J. Jilin Univ. Earth Sci. Ed.* 54 (03), 840–861. doi:10.13278/j.cnki.jjuese.20230345